Lattice vibrations in time-fluctuating percolation networks: Application to Brillouin scattering from glasses and liquids

R. Granek
*Theory of Condensed Matter, Cavendish Laboratory, Madingley Road, Cambridge, CB3 0HE, United Kingdom**
and School of Chemistry, Sackler Faculty of Exact Sciences, Tel-Aviv University, Tel-Aviv 69978, Israel
(Received 21 June 1991)

A model of lattice vibrations in a percolation network which is stochastically fluctuating in time is treated within the effective-medium approximation (EMA). This work generalizes previous studies on vibrations in static percolation networks, which are characterized by phonon-fracton crossover, to the dynamical regime. Our result for the frequency-dependent effective force constant $K(\omega)$ is that it depends on ω through the combinations $\omega - i\tau_j^{-1}$, where τ_j are the matrix fluctuation times. For a single-exponential relaxation, we obtain the relation $K(\omega,\tau^{-1}) = K_0(\omega - i\tau^{-1})$, where K_0 is the effective force constant of the static ($\tau^{-1}=0$) medium. We calculate the effect of lattice renewal on the dispersion relation and on the dynamical structure factor, for which we analyze separately the frequency-dependent linewidth and sound velocity. For the latter quantities, we also provide scaling *Ansätze*, which are shown to be obeyed by the EMA for sufficiently small fluctuation times τ. We find that the dynamic fluctuation effects become dominant for small enough τ and are manifested (as τ decreases) first as a nonuniform broadening and later as a "motional narrowing" of the dynamical structure factor line. The implications of our results on Brillouin scattering from glass-forming polymer melts and polymer electrolytes are discussed.

I. INTRODUCTION

The mechanical properties of random networks have been the subject of many theoretical and experimental studies in recent years, mainly in conjunction with so-called phonon-fracton model.[1-20] These studies deal with systems which are fractal below a certain correlation length ξ (with either mass or bond fractality) and that are homogeneous for length scales much larger than ξ. The vibrational eigenstates in such systems have been argued to be strongly localized for frequencies larger than a certain crossover frequency ω_{co} and extended (or, more accurately, weakly localized) for frequencies below ω_{co}. For scalar elasticity, ω_{co} is related to ξ by[1-3,7]

$$\omega_{co} \sim \xi^{-(1+\theta/2)} , \tag{1}$$

where θ is the anomalous diffusion exponent (where $\langle r^2(t)\rangle \sim t^{2/(2+\theta)}$ for $r \ll \xi$ or for times $t \ll \xi^{(2+\theta)2}$). The results of this behavior show up in crossovers in the density of states,[1-3,7] $N(\omega)$ (which in turn influences other observables such as the specific heat),[3,12] in the dispersion relation $\omega(\Lambda)$, and in the dynamical structure factor[6] $S(q,\omega)$ (with $q = 2\pi/\Lambda$ being the wave vector). The latter can be written in a quasi-Lorentzian form,[6] giving rise to the introduction of two other quantities: the frequency-dependent linewidth $\Gamma(\omega)$, which may be interpreted as the inverse phonon lifetime (or relaxation time), and the frequency-dependent sound velocity $c_s(\omega)$.

The density of states for $\omega \gg \omega_{co}$ (the fracton regime) in d dimensions is given by[1-3,7]

$$N(\omega) \sim \omega^{\tilde{d}-1} , \tag{2}$$

where $\tilde{d}$ is called the fracton dimension. For $\omega \ll \omega_{co}$ (the phonon regime), it is phononlike:[7]

$$N(\omega) \sim \omega_{co}^{\tilde{d}-d}\omega^{d-1} . \tag{3}$$

The fracton dimension $\tilde{d}$ is related to the fractal dimension $\bar{d}$ and to the anomalous diffusion exponent θ by[1]

$$\tilde{d} = 2\bar{d}/(2+\theta) . \tag{4}$$

The dispersion relation for wavelengths $\Lambda \gg \xi$ (the phonon regime) is[1]

$$\omega_{ph}(\Lambda) \sim c_s \Lambda^{-1} , \tag{5}$$

where the sound velocity c_s is related to ξ by

$$c_s \sim \xi^{-\theta/2} , \tag{6}$$

while in the fracton regime $\Lambda \ll \xi$, it is

$$\omega_{fr}(\Lambda) \sim \Lambda^{-(1+\theta/2)} . \tag{7}$$

It has also been argued that the Brillouin linewidth $\Gamma(\omega)$ (or the inverse phonon relaxation time) behaves as[6,8]

$$\Gamma(\omega) \sim \omega_{co}^{-d}\omega^{d+1}, \quad \omega \ll \omega_{co} , \tag{8}$$

obeying the Rayleigh scattering law [$\Gamma(\omega) \sim \omega^4$ in three dimensions), while in the fracton regime it obeys the Ioffe-Regel localization criterion[6,8]

$$\Gamma(\omega) \sim \omega, \quad \omega \gg \omega_{co} . \tag{9}$$

Finally, the frequency-dependent sound velocity in the two regimes was shown[6] to satisfy

$$c_s(\omega) \sim \omega_{co}^{\theta/(2+\theta)} \text{ for } \omega \ll \omega_{co} , \tag{10}$$

$$c_s(\omega)\sim\omega^{\theta/(2+\theta)} \text{ for } \omega\gg\omega_{co} . \quad (11)$$

Since the percolation network is fractal below the percolation correlation length ξ, which diverges at the percolation threshold p_c as $\xi\sim(p-p_c)^{-\nu}$, all the above results apply to it. The effective-medium approximation (EMA) for a percolation network yields (for dimensionality $2<d<4$) the following results for the exponents:[4-6]

$$\theta=2, \quad \bar{d}=2, \quad \tilde{d}=1 . \quad (12)$$

Numerical values for these exponents (in a percolation network) are[1,21(a)]

$$\theta=0.80, \quad \bar{d}=1.9, \quad \tilde{d}=1.36 \text{ for } d=2 \quad (13)$$

and

$$\theta=1.55, \quad \bar{d}=2.5, \quad \tilde{d}=1.42 \text{ for } d=3 . \quad (14)$$

Alexander and Orbach[1] have conjectured that $\tilde{d}=\frac{4}{3}$ for all $d\geq 2$, although it was shown to break down very weakly[21(b)] for dimensionality $d<6$ (as also implied by the above values). Conversely, Aharony *et al.*[8] argued that Eq. (9) applies for the phonon-fracton problem only if the Alexander-Orbach conjecture is exact. Recent simulations[11] for the vibrational density of states on a percolating network support $\tilde{d}=\frac{4}{3}$.

From the experimental point of view, results of the phonon-fracton model are fairly successful in explaining the low-temperature behavior of glasses, via specific-heat and thermal-conductivity measurements.[2,3,12,19] In particular, the non-Debye behavior of the heat capacity,[12] found in epoxy resins above 8 K, and the plateau in the thermal conductivity[12] between 8 and 15 K are an immediate consequence of the model. Less trivial is the linear dependence on temperature of the thermal conductivity[19] above 15 K, which has also been confirmed by experiment.[19,22] Thus the phonon-fracton model seems to be able to explain some universal features of glasses at low temperature.

Dynamic measurements for verifying the phonon-fracton model have been carried out, however, mainly on silica aerogels.[13-17] These are specially prepared materials formed by aggregation and intensive drying processes, which are needed to create the mass fractal structure. In these materials small-angle x-ray-scattering measurements[14,15] have shown that the structure is mass fractal within a certain correlation length. When combined with the x-ray measurements, the measured density of states[16] and dynamical structure factor[13,15,17] support the phonon-fracton model.

When applied to glasses, a word of caution should be given since the phonon-fracton model relies on the fractal structure of the network. (In fact, other explanations for the behavior of the density of states in glasses have been suggested.[23]) Fractality is not the common picture for glasses, even if one considers only fractal force constants with the mass distribution taken to be homogeneous. Indeed, a more appropriate picture of vitreous silica[24] is that of topological disorder. Yet the fractal picture seems to be suitable for cross-linked polymer networks (such as epoxy resins[25]), where the fractality of the chemical bond structure (i.e., the force constants) is a direct consequence of the nature of the polymer.[26] Indeed, the phonon-fracton model was partially confirmed in epoxy resins[18] and other amorphous polymers[27] by dynamical measurements. A more general attitude is just to define a correlation length for disorder that leads to strongly localized eigenstates for ω above ω_{co}. One can then consider the fractal as a convenient model that generates strongly localized eigenstates.

With this in mind, we address the consequences of the glass transition. Below the glass transition, the system is frozen and therefore one deals with static disorder, but as the temperature is raised above the transition, the rearrangements that occur via matter diffusion may affect both the phonon and fracton lifetime and dispersion law. In Brillouin scattering[28] from glass-forming liquids, performed well above the glass transition, the width of the phonon peak shows a universal behavior as a function of the temperature, the width going through a maximum at some temperature. Such a behavior is also found in more simple fluids (termed as "complex" in the past) such as CS_2,[29] CCl_4,[30] and glycerol.[31] Although the well-known theory of Mountain[32,33] (and Montrose, Solovyev, and Litovitz[34]) seems to explain this behavior, this theory was originally meant to apply to these "simple" fluids (by the current terminology). Yet it has also been extensively used for glasses[28,35] (in a purely phenomenological manner), while it seems inadequate to treat cross-linked polymers as liquids; they are much more like solids.

The purpose of the present study is to link Brillouin-scattering measurements performed well above the glass transition[28] to measurements in the glassy state as the system is taken continuously through the transition. As a convenient mathematical description, we choose the percolation network, which is fractal on length scales much smaller than the percolation correlation length (and much larger than the lattice spacing). We do not mean that amorphous polymer networks can be viewed as percolation networks. The main point is the expected fractal nature of these materials for distances below the average "cross-linking" distance.

In recent years dynamic bond percolation theories for diffusion have been developed.[36-39] The work of Druger and co-workers[36] was motivated by conductivity measurements in polymer electrolytes which show strong coupling to other observables such as viscosity, Brillouin scattering, and NMR relaxation. A similar microscopic model for vibrations in these materials (as presented in the present study) is equally important. Both theories use the percolation model and use a microscopic rearrangement (or relaxation) time τ that controls the evolution of the disorder.

In the present study, we use the effective-medium approximation[40-43,38,39] to obtain an analytic continuation rule for the effective force constant, which is similar to that found for the diffusion constant in the analogous diffusion problem. The formalism used here is merely a generalization of the Harrison-Zwanzig[38] treatment and its Granek-Nitzan extensions[39] to the scalar vibrational problem.

Our starting point is then the (infinite) set of stochastic

equations of motion for the displacement component $U_i(t)$ (i is the site index) based on the scalar elasticity model,

$$\frac{d^2}{dt^2}U_i(t)=\omega_0^2\sum_{j\in\{i\}}\sigma_{ij}(t)[U_j(t)-U_i(t)]\ , \tag{15}$$

where $\{i\}$ is the set of nearest-neighbor sites to i, ω_0 is the natural spring frequency, and $\sigma_{ij}(t)$ are stochastic variables, which will be taken to fluctuate (at equilibrium) between 0 or 1 according to the rate equation[38]

$$\frac{\partial}{\partial t}\begin{bmatrix}\phi_\alpha(0,t)\\ \phi_\alpha(1,t)\end{bmatrix}=\frac{1}{\tau}\begin{bmatrix}-p & 1-p\\ p & -(1-p)\end{bmatrix}\begin{bmatrix}\phi_\alpha(0,t)\\ \phi_\alpha(1,t)\end{bmatrix}\ . \tag{16}$$

Here $\phi_\alpha(\sigma_\alpha,t)$ is the probability that the bond $\alpha=(ij)$ has the value σ_α at time t, p is the average fraction of open bonds ($\sigma_{ij}=1$) at any time (and the fraction of time that a specific bond is open during an infinitely long period), and τ is the fluctuation time. Both p and τ are assumed to be independent of the U_i's. Thus we assume that each bond fluctuates independently of the local strain U_j-U_i and independently of all other bonds. Both assumptions are not entirely physical, but for simplicity we disregard this aspect of the problem for now. For the same reason, we shall limit ourselves to the scalar elasticity model,[44–46] although tensorial effects were shown to result with[47] $\bar{d}<1$ (which is significant for the behavior of the density of states for $\omega>\omega_{co}$).

Our objective is then to average over the equations of motion (15) in conjunction with Eq. (16). In Sec. II it is shown that the averaged equations of motion are non-Newtonian and (quite) generally can be written in an effective-medium form

$$\frac{d^2}{dt^2}\langle U_i(t)\rangle=\omega_0^2\sum_{j\in\{i\}}\int_0^t dt'\,\tilde{K}(t-t')[\langle U_j(t')\rangle-\langle U_i(t')\rangle]\ , \tag{17}$$

implying a microscopic viscoelastic behavior. The problem still remains to determine the effective force constant $\tilde{K}(t)$. A solution for this problem is obtained within the EMA in Sec. II. In Secs. III and IV, we examine the implications of the time-dependent bond fluctuations in the binary percolation model on the dispersion relation and on the dynamical structure factor. Some predictions for glass-forming polymers and (solvent-free) polymer electrolytes are provided in Sec. V. We summarize our results in Sec. VI.

II. GENERAL FORMALISM AND EFFECTIVE-MEDIUM APPROXIMATION

To make the formalism applicable to more complicated fluctuation processes than the one described by Eq. (16), we allow (more generally) for many values for the bond force constant σ_α. Following the basic formalism used by Harrison and Zwanzig[38] and by Granek and Nitzan[39] for the analogous diffusion problem, we denote by $\phi_\alpha(\sigma_\alpha,t)$ the probability that bond α has the value σ_α at time t and assume it to obey the master equation[39]

$$\frac{\partial}{\partial t}\phi_\alpha(\sigma,t)=\sum_{\sigma'}\Omega_\alpha(\sigma,\sigma')\phi_\alpha(\sigma',t)\equiv\hat{\Omega}_\alpha\phi_\alpha(\sigma,t)\ , \tag{18}$$

which defines the operator $\hat{\Omega}_\alpha$. The equilibrium solution of Eq. (18), $\rho_\alpha(\sigma_\alpha)$, is the solution of

$$\sum_{\sigma'}\Omega_\alpha(\sigma,\sigma')\rho_\alpha(\sigma')=0\ . \tag{19}$$

The set of Eqs. (15) can be written in the vector form (henceforth we set $\omega_0=1$; hence all timescales will be given in units of ω_0^{-1})

$$\begin{aligned}&\frac{d}{dt}\mathbf{U}=\mathbf{P}\ ,\\ &\frac{d}{dt}\mathbf{P}=-\mathbf{W}\cdot\mathbf{U}\equiv-\sum_\alpha\sigma_\alpha(t)\mathbf{V}_\alpha\cdot\mathbf{U}\ ,\end{aligned} \tag{20}$$

where α corresponds to a bond (ij) between the nearest-neighbor sites i and j and where

$$\mathbf{V}_\alpha=(|i\rangle-|j\rangle)(\langle i|-\langle j|) \tag{21}$$

and

$$\mathbf{U}=\sum_i U_i|i\rangle,\quad \mathbf{P}=\sum_i P_i|i\rangle \tag{22}$$

(with $\langle i|j\rangle=\delta_{ij}$).

To obtain the average equations (17), we start with the Liouville master equation for the joint probability distribution $f(\mathbf{U},\mathbf{P},\vec{\sigma},t)$, to find (at time t) the displacements and momenta given by $\mathbf{U}$ and $\mathbf{P}$ and the bonds in the collective state $\vec{\sigma}=(\sigma_1,\sigma_2,\ldots,\sigma_\alpha,\ldots)$,

$$\frac{\partial}{\partial t}f=\frac{\partial}{\partial\mathbf{P}}\cdot(\mathbf{W}\cdot\mathbf{U}f)-\frac{\partial}{\partial\mathbf{U}}\cdot(\mathbf{P}f)+\hat{\Omega}f\ , \tag{23}$$

where

$$\hat{\Omega}=\sum_\alpha\hat{\Omega}_\alpha\ . \tag{24}$$

If $\hat{\Omega}=0$ in Eq. (23), this is just the usual Liouville equation for the equations of motion (20). As initial conditions, we assume that both the displacements and momenta have specific but arbitrary values $\mathbf{U}_0$ and $\mathbf{P}_0$, respectively, while the bonds are distributed according to their *equilibrium* distribution. Hence we limit our analysis to the effect of bond fluctuations at equilibrium. The initial condition for $f(\mathbf{U},\mathbf{P},\vec{\sigma},t)$ is therefore

$$f(\mathbf{U},\mathbf{P},\vec{\sigma},t=0)=\delta(\mathbf{U}-\mathbf{U}_0)\delta(\mathbf{P}-\mathbf{P}_0)\rho(\vec{\sigma})\ , \tag{25}$$

where $\rho(\vec{\sigma})$ is the equilibrium distribution for the collective bond state and is given by

$$\rho(\vec{\sigma})=\prod_\alpha\rho_\alpha(\sigma_\alpha)\ . \tag{26}$$

We perform the needed average in two stages. First, the partial average of an observable $\mathbf{A}$ is defined as

$$\mathbf{A}(\vec{\sigma},t)=\int d\mathbf{U}\int d\mathbf{P}\ \mathbf{A}f(\mathbf{U},\mathbf{P},\vec{\sigma},t)\ . \tag{27}$$

The full average of $\mathbf{A}$ is then given by $\sum_{\vec{\sigma}}\mathbf{A}(\vec{\sigma},t)$. With $\mathbf{A}$ being $\mathbf{U}$ and $\mathbf{P}$, we get from Eq. (23), using integration by parts [and the fact that $f(\mathbf{U},\mathbf{P},\vec{\sigma},t)$ should vanish faster than any power of $\mathbf{U}$ or $\mathbf{P}$ at the boundaries of the $(\mathbf{U},\mathbf{P})$ phase space],

$$\frac{\partial}{\partial t}\mathbf{P}(\vec{\sigma},t)=-\mathbf{W}\cdot\mathbf{U}(\vec{\sigma},t)+\hat{\Omega}\mathbf{P}(\vec{\sigma},t)\ ,$$
$$\frac{\partial}{\partial t}\mathbf{U}(\vec{\sigma},t)=\mathbf{P}(\vec{\sigma},t)+\hat{\Omega}\mathbf{U}(\vec{\sigma},t)\ . \tag{28}$$

By Eqs. (27) and (25), we have, for the initial conditions,

$$\mathbf{P}(\vec{\sigma},t=0)=\mathbf{P}_0\rho(\vec{\sigma}),\quad \mathbf{U}(\vec{\sigma},t=0)=\mathbf{U}_0\rho(\vec{\sigma})\ . \tag{29}$$

We now take the Laplace transform [denoting by $\mathbf{A}(\vec{\sigma},z)$ the transform of $\mathbf{A}(\vec{\sigma},t)$] of Eqs. (28) and solve for $\mathbf{P}(\vec{\sigma},z)$ and $\mathbf{U}(\vec{\sigma},z)$. In this procedure it is essential to keep the order of noncommuting quantities. The procedure is given in detail in Appendix A. We obtain

$$\begin{bmatrix}\mathbf{P}(\vec{\sigma},z)\\ \mathbf{U}(\vec{\sigma},z)\end{bmatrix}=\begin{bmatrix} z\mathbf{g}(\vec{\sigma},z) & z^2\mathbf{g}(\vec{\sigma},z)-\rho(\vec{\sigma})\mathbf{1}\\ z(z-\hat{\Omega})^{-1}\mathbf{g}(\vec{\sigma},z) & z^2(z-\hat{\Omega})^{-1}\mathbf{g}(\vec{\sigma},z)\end{bmatrix}\cdot\begin{bmatrix}\mathbf{P}_0\\ \mathbf{U}_0\end{bmatrix}\ , \tag{30}$$

where we have defined the partially averaged Green's operator $\mathbf{g}(\vec{\sigma},z)$ as

$$\mathbf{g}(\vec{\sigma},z)=[(z-\hat{\Omega})^2\mathbf{1}+\mathbf{W}(\vec{\sigma})]^{-1}\rho(\vec{\sigma})\ . \tag{31}$$

To obtain Eq. (30), we have explicitly used $\hat{\Omega}\rho(\vec{\sigma})=0$. Thus Eq. (30) is valid only when $\rho(\vec{\sigma})$ is indeed taken as the *equilibrium* distribution of the bonds. The full averages of P and U are therefore given by

$$\begin{bmatrix}\langle\mathbf{P}(z)\rangle\\ \langle\mathbf{U}(z)\rangle\end{bmatrix}=\begin{bmatrix} z\mathbf{g}(z) & z^2\mathbf{g}(z)-1\\ \mathbf{g}(z) & z\mathbf{g}(z)\end{bmatrix}\cdot\begin{bmatrix}\mathbf{P}_0\\ \mathbf{U}_0\end{bmatrix}\ , \tag{32}$$

where we have defined $\mathbf{g}(z)$ as

$$\mathbf{g}(z)=\sum_{\vec{\sigma}}\mathbf{g}(\vec{\sigma},z) \tag{33}$$

(i.e., the fully averaged Green's operator). To get Eq. (32), we have used the fact that $\hat{\Omega}$ has the property $\sum_{\vec{\sigma}}\Omega(\vec{\sigma},\vec{\sigma}')=0$ and the normalization condition $\sum_{\vec{\sigma}}\rho(\vec{\sigma})=1$. Thus we have reduced the averaging to a calculation of one quantity $\mathbf{g}(z)$. We now write $\mathbf{g}(z)$ in the form

$$\mathbf{g}(z)=[z^2\mathbf{1}+\mathbf{W}_m(z)]^{-1}\ , \tag{34}$$

where

$$\mathbf{W}_m(z)=K(z)\sum_{\alpha}\mathbf{V}_\alpha\ . \tag{35}$$

Here the effective force constant $K(z)$ is yet undetermined. In Eqs. (34) and (35) we have invoked the effective-medium assumption that an analytical function $K(z)$, which makes Eqs. (33) and (34) exactly equal, indeed exists. Upon inversion of Eq. (32), with Eqs. (34) and (35), the averaged equations of motion become the non-Newtonian equations (17) [with $\tilde{K}(t)$ being the inverse Laplace transform of $K(z)$].

To find $K(z)$ we use the EMA. In the EMA,[38,39] one considers a medium consisting of one fluctuating bond (σ_1) embedded in an otherwise effective medium with bond force constants $K(z)$. Therefore $\mathbf{W}$ and $\hat{\Omega}$ for this medium are given by

$$\mathbf{W}=K(z)\sum_{\alpha(\neq 1)}\mathbf{V}_\alpha+\sigma_1\mathbf{V}_1=\mathbf{W}_m+[\sigma_1-K(z)]\mathbf{V}_1\ , \tag{36}$$

$$\hat{\Omega}=\hat{\Omega}_1\ . \tag{37}$$

Using Eqs. (36), (37), and (31), we obtain a self-consistent condition for the effective force constant,

$$[z^2\mathbf{1}+\mathbf{W}_m(z)]^{-1}=\sum_{\sigma_1}\mathbf{\Gamma}_{\sigma_1}\ , \tag{38}$$

with

$$\mathbf{\Gamma}_{\sigma_1}=[(z-\hat{\Omega}_1)^2\mathbf{1}+\mathbf{W}_m+(\sigma_1-K)\mathbf{V}_1]^{-1}\rho_1(\sigma_1)\ . \tag{39}$$

The remaining part of the procedure follows exactly the lines of the EMA for the effective diffusion coefficient.[38,39] Here we quote only the result. Similar to the diffusion problem, the effective force constant is determined from the requirement that the determinant of coefficients of $\mathbf{Q}_\sigma$ (which are vectors in the site space) in the $n+1$ equations below (n is the number of bond states) vanishes:

$$\sum_{\sigma}(\sigma-K)\mathbf{Q}_\sigma=\mathbf{0} \tag{40}$$

and

$$\sum_{\sigma}M_\sigma^l[1+(\sigma-K)h_l]\mathbf{Q}_\sigma=\mathbf{0},\quad \lambda_l\neq 0,\quad l=1,2,\ldots,n\ , \tag{41}$$

where M_σ^l are elements of the left eigenvector of the transition matrix Ω_α with nonzero eigenvalue $-\lambda_l(\sum_{\sigma'}M_{\sigma'}^l\Omega_\alpha(\sigma',\sigma)=-\lambda_l M_\sigma^l)$,

$$h_l=\frac{p_c}{K}[1-\epsilon_l g(\epsilon_l)]\ , \tag{42}$$

with $g(\epsilon)$ being the lattice Green's function of the origin (Appendix B),

$$\epsilon_l=\frac{(z+\lambda_l)^2}{K}\ , \tag{43}$$

and $p_c=2/Z$ is the static EMA percolation threshold (with Z being the coordination number of the underlying lattice). The result for $K(z)$ differs from the EMA result for the diffusion coefficient[38,39] only by the definition of the spectral variables ϵ_l, with $(z+\lambda_l)^2$ replacing $z+\lambda_l$. Note that $K(z)$ depends on z only through the combinations $z+\lambda_l$. The result for $K(z)$ is rather complicated when several bond states are assumed to be present. In the next sections, we therefore discuss in detail the binary-value model ($\sigma=0,1$), for which the result is simple and the static case has been studied extensively.

III. BINARY DISTRIBUTION AND THE DISPERSION RELATION

In the Harrison-Zwanzig fluctuation model[38] (originally solved for the diffusion model), the bond dynamics is described by the 2×2 master equation (16) for which the equilibrium solution is $\rho(1)=p$, $\rho(0)=1-p$. Applying the above formalism, using $z=i\omega+0$ for analytic continuation to the complex plane, yields the EMA result

$$K=\frac{p-p_c+p_c\varepsilon g(\varepsilon)}{1-p_c+p_c\varepsilon g(\varepsilon)} , \tag{44}$$

with

$$\varepsilon=\frac{(i\omega+\tau^{-1})^2}{K} \tag{45}$$

(which reduces to the result of Refs. 4–6 for $\tau^{-1}=0$). This implies that, in the single bond EMA, the frequency-dependent effective force constant for the dynamic case, $K(\omega,\tau^{-1})$, is related to that for the static case, $K_0(\omega)$, by the analytical continuation rule

$$K(\omega,\tau^{-1})=K_0(\omega-i\tau^{-1}) . \tag{46}$$

Following Refs. 4–6, we now turn to examine $K(\omega)$ near the static percolation threshold and for low frequencies and slow renewal (small τ^{-1}), namely, where $\omega,\tau^{-1}\sim p-p_c\ll1$. Consider first the static case $\tau^{-1}=0$. For $2<d<4$, we can use,[48] to first order, $g(\varepsilon)\simeq g(0)$, which is a finite numerical constant. This leads to

$$K\simeq\frac{p-p_c+[(p-p_c)^2-4(1-p_c)p_c g(0)\omega^2]^{1/2}}{2(1-p_c)} . \tag{47}$$

It is seen from Eq. (47) that as ω increases from zero, $K'\equiv\mathrm{Re}K$ decreases. For $\omega<\omega_{co}$, where

$$\omega_{co}^2=\frac{(p-p_c)^2}{4g(0)p_c(1-p_c)} , \tag{48}$$

K is real (in this approximation). For $\omega>\omega_{co}$ the imaginary part of K is finite and increases as $(\omega^2-\omega_{co}^2)^{1/2}$. The "nonanalyticity" that appears at ω_{co} leads to a hump in the density of states[5] (and in the dynamic structure factor[6]) at the phonon-fracton crossover $\omega\sim\omega_{co}$. As τ^{-1} increases from zero, we find that this sharp transition becomes smoother and shifts to

$$\omega_c^2\simeq\omega_{co}^2+\tau^{-2} . \tag{49}$$

We now turn to analyze the dispersion relation (in the Debye approximation), namely, the relation between frequency and wave vector q (for small q, $q=|\mathbf{q}|$). $\omega(q)$ can be obtained by solving

$$\omega^2(q)=K(\omega(q))q^2 , \tag{50}$$

in conjunction with the effective-medium equation (44). Focusing on the regime $\omega,\tau^{-1}\sim p-p_c\ll1$, we can make use[48] of the asymptotic expansion[5] for $g(\varepsilon)$ near $\varepsilon=0$ (for $2<d<4$),

$$g(\varepsilon)\simeq g(0)-\chi_d\varepsilon^{d/2-1} , \tag{51}$$

where $g(0)$ and χ_d are numerical constants. [For a three-dimensional sc lattice, $g(0)=0.252\,73$ and $\chi_3=1/4\pi$.] Substituting $K=\omega(q)/q^2$ and

$$\omega(q)=\omega_q+i\delta_q \tag{52}$$

in Eq. (44), we obtain equations for ω_q and δ_q.

It can be shown that a crossover behavior in the dispersion relation appears at a certain wave vector $q=q_c$. For $\tau^{-1}=0$, this q_c has been obtained by Entin-Wohlman *et al.*[4] to be [denoting $q_{c0}\equiv q_c(\tau^{-1}=0)$]

$$q_{c0}^2=\frac{p-p_c}{g(0)p_c} . \tag{53}$$

In fact, we expect that[4] $q_{c0}\sim\xi^{-1}$, where ξ is the percolation correlation length; Eq. (53) therefore implies that $\xi\sim(p-p_c)^{1/2}$ in the EMA. For $\tau^{-1}\neq0$ (but small) and above the percolation threshold, this crossover is changed to

$$q_c\simeq q_{c0}\left[1+\frac{d|\chi_d^{(2)}|(1-p_c)^{1/2}}{2g(0)^{(d-1)/2}p_c^{(d-3)/2}(p-p_c)^{2-d/2}}\tau^{-1}\right] , \tag{54a}$$

where

$$\chi_d^{(1)}+i\chi_d^{(2)}=(-1)^{d/2}\chi_d . \tag{54b}$$

Thus q_c increases as τ^{-1} increases from zero.

In the small-q limit $q\ll q_c$, the dispersion relation is phonon like $\omega_q\simeq c_s q$, where the sound velocity c_s for large τ behaves asymptotically as

$$c_s\simeq\left[\frac{p-p_c}{1-p_c}\right]^{1/2}\left[1+\frac{g(0)p_c(1-p_c)}{2(p-p_c)^2}\tau^{-2}+\cdots\right] \quad \text{for } p>p_c \text{ and } \tau^{-1}\ll\omega_{co}\ll1 , \tag{55}$$

$$c_s\simeq\left[\frac{p_c g(0)}{1-p_c}\right]^{1/4}\tau^{-1/2} \quad \text{for } p=p_c \text{ or } \omega_{co}\ll\tau^{-1}\ll1 , \tag{56}$$

$$c_s\simeq\left[\frac{p_c g(0)}{p_c-p}\right]^{1/2}\tau^{-1} \quad \text{for } p<p_c \text{ and } \tau^{-1}\ll\omega_{co}\ll1 , \tag{57}$$

where $\omega_{co} \sim p - p_c$ [cf. Eq. (48)]. It is seen from Eq. (55) that the sound velocity c_s starts to change considerably as τ^{-1} increases from zero only when $\tau\omega_{co} \sim 1$. Note that this condition is the same as the condition for a considerable change in the crossover frequency $\omega_c(\tau^{-1})$ in Eq. (49).

In the phonon regime $q \ll q_c$ but when q also obeys $q \gg (\tau c_s)^{-1}$ (implying $p > p_c$ and $\tau^{-1} q_{c0}^{-1} \ll q \ll q_{c0}$), δ_q approaches the asymptotic form

$$\delta_q \simeq -\frac{p_c}{2(1-p_c)^{1/2}(p-p_c)^{1/2}} \left[\chi_d^{(2)} q^{d+1} - d\chi_d^{(1)} q^d \left[\frac{1-p_c}{p-p_c} \right]^{1/2} \tau^{-1} + (\chi_d^{(2)} - d\chi_d^{(1)}) dq^{d-1} \frac{1-p_c}{2(p-p_c)} \tau^{-2} \right] + \frac{p_c g(0)}{p-p_c} q^2 \tau^{-1} + \cdots . \quad (58)$$

Thus δ_q increases with τ^{-1}; namely, the (dynamic) fluctuations decrease the phonon lifetime. This effect adds to the relaxation caused by scattering from effective "defects," which can model the strong spatial disorder in this long-wavelength regime. Indeed, for a static network[4] ($\tau^{-1}=0$), $\delta_q \sim q^{d+1}$, which is the well-known Rayleigh-scattering[49,50] law (for scattering of phonons from defects). Equation (58) shows that the increase of the lifetime of a phonon with increasing wavelength is maintained for a fluctuating network. For $q \ll (\tau c_s)^{-1}$, δ_q shows a crossover to a different behavior, which will not be discussed here.

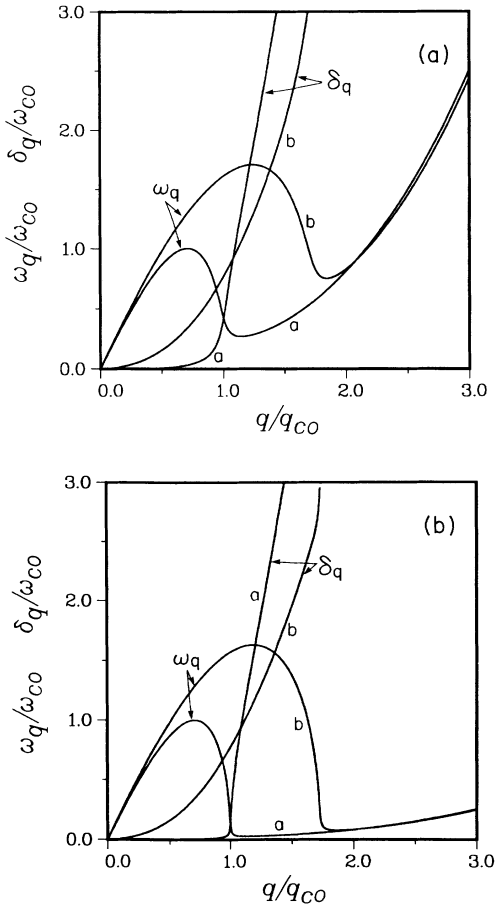

FIG. 1. Real and imaginary parts of the dispersion relation (normalized by ω_{co}^{-1}), ω_q/ω_{co} and δ_q/ω_{co}, vs the reduced wave vector q/q_{c0} for two values of p: (a) $(p-p_c)/(1-p_c)=10^{-2}$ and (b) $(p-p_c)/(1-p_c)=10^{-4}$. The static case $\tau=\infty$ (the lines denoted by *a*) and one dynamic case $\tau^{-1}>0$ (the lines denoted by *b*) are shown in each figure: (a) $\tau=100$ and (b) $\tau=10^4$.

The numerical solution for ω_q and δ_q (for $d=3$) is depicted in Fig. 1. We plot ω_q/ω_{co} and δ_q/ω_{co} versus q/q_{c0} for two values of p, $(p-p_c)/(1-p_c)=10^{-2}$ [Fig. 1(a)] and $(p-p_c)/(1-p_c)=10^{-4}$ [Fig. 1(b)], both for the static case $\tau=\infty$ and for two values of fluctuation time, $\tau=100$ [Fig. 1(a)] and $\tau=10^4$ [Fig. 1(b)]. It is evident from these figures that there is a characteristic cutoff wave vector q_c separating the two regimes, $q<q_c$ and $q>q_c$. It is also seen that for $\tau^{-1}>0$, q_c is roughly the same as q_{c0} [$\equiv q_c(\tau^{-1}=0)$], although a little larger, as implied by Eq. (54). The same is true for the crossover frequency ω_c and the sound velocity c_s: ω_c, which is the local maximum in ω_q versus q, and the sound velocity, c_s, which is the slope of ω_q versus q as $q \to 0$, are seen to increase with τ^{-1} as implied by Eqs. (49) and (55).

For $\tau^{-1}=0$ and $q<q_c$, δ_q is relatively small (because $\delta_q \sim q^4$), while for $q>q_c$, δ_q increases rapidly ($\delta_q \sim q$). Thus, if a phonon of wave vector q is excited (by some mechanism), it will relax quickly (with a relaxation rate δ_q). This is just another manifestation of the fact that the eigenmodes of such "short" wavelengths (namely, the fractons) are really strongly localized and is further discussed in Sec. IV. As τ^{-1} increases, δ_q in the phonon regime $q<q_c$ increases, as implied by Eq. (55). However for $q>q_c$, δ_q is somewhat decreased by the fluctuation process. The latter fact may be interpreted as a result of a "smearing out" of the fractals (whose effective linear size is the percolation correlation length).

IV. DYNAMICAL STRUCTURE FACTOR

A. General results

Here we consider the inelastic one-phonon term of the dynamical structure factor (e.g., light- or neutron-scattering intensities). With the common assumption of self-averaging and within scalar elasticity, it is possible to write the scattered light intensity in the form (see Appendix C)

$$\frac{d^2\sigma_1}{d\Omega\, dE} = -Ne^{-2W}[n(\omega)+1]\frac{q^2}{\pi} \times \mathrm{Im} \sum_j e^{-i\mathbf{q}\cdot\mathbf{R}_{ij}} g_{ij}(i\omega+0) . \quad (59)$$

Here W is the Debye-Waller factor,

$$2W=q^2\langle U(0)^2\rangle_T \ , \tag{60}$$

and $n(\omega)$ is the Bose population factor,

$$n(\omega)=(e^{\beta\hbar\omega}-1)^{-1} \ , \tag{61}$$

with $\beta=1/k_BT$; $\mathbf{R}_{ij}=\mathbf{R}_j-\mathbf{R}_i$ is the vector separation between sites i and j, $g_{ij}(z)$ are elements of the fully averaged Green's operator of the theory of Sec. II [Eqs. (33) and (34)], and N is the number of scatterers.

We now leave out the thermal factors[51] and define the dynamical structure factor as[6]

$$S(\mathbf{q},\omega)=2\,\mathrm{sgn}(\omega)\mathrm{Im}G(\mathbf{q},\omega-i0) \ , \tag{62}$$

where

$$G(\mathbf{q},\omega-i0)=-\sum_j e^{-i\mathbf{q}\cdot\mathbf{R}_{ij}}g_{ij}(z=i\omega+0) \ . \tag{63}$$

In a simple cubic lattice in d dimensions, $G(\mathbf{q},\omega)$ is given by[44] ($-\pi<q_\delta<\pi$)

$$G(\mathbf{q},\omega)=\left[\omega^2-2K\sum_{\delta=1}^{d}(1-\cos q_\delta)\right]^{-1} \ , \tag{64}$$

where q_δ are the components of the vector $\mathbf{q}$. In the Debye approximation ($q\ll1$),

$$2\sum_\delta(1-\cos q_\delta)\simeq q^2 \tag{65}$$

($q=|\mathbf{q}|$), and with $K=K'+iK''$, Eqs. (62) and (64) yield[6]

$$S(q,\omega)=\frac{2q^2\mathrm{sgn}(\omega)K''}{\omega^4-2\omega^2q^2K'+q^4|K|^2} \ . \tag{66}$$

Equation (66) may be rewritten in the form[6]

$$S(q,\omega)=\mathrm{sgn}(\omega)[S_+(q,\omega)-S_-(q,\omega)] \ , \tag{67}$$

$$S_\pm(q,\omega)=\frac{c_s(\omega)q}{\omega^2}\,\frac{\Gamma(\omega)}{[\omega\pm c_s(\omega)q]^2+\Gamma(\omega)^2} \ , \tag{68}$$

where the frequency-dependent sound velocity is given by

$$c_s(\omega)=\frac{|K(\omega)|}{\mathrm{Re}\sqrt{K(\omega)}} \tag{69}$$

and the frequency-dependent linewidth is

$$\Gamma(\omega)=\omega\frac{\mathrm{Im}\sqrt{K(\omega)}}{\mathrm{Re}\sqrt{K(\omega)}} \ . \tag{70}$$

As expected, the one-phonon structure factor shows two quasi-Lorenzian peaks, one for phonon emission with energy $\hbar\omega=\hbar c_s(\omega)q$ and the other for phonon absorption with the same energy.[52]

Equations (66) or (67)–(70) allow one to calculate $S(q,\omega)$ given an expression for $K(\omega)$. The time-reversal symmetry of the correlation function $\langle U_i(0)U_j(t)\rangle$ in Eq. (C2) implies that $S(q,\omega)$ should be a symmetric function of ω. This requirement leads to the following relations under the symmetry operation $\omega\to-\omega$: $K'(\omega,\tau^{-1})=K'(-\omega,\tau^{-1})$ and $K''(\omega,\tau^{-1})=-K''(-\omega,\tau^{-1})$. Indeed, the EMA expression for $K(\omega)$ obeys these symmetry properties, as can be shown using the general expression for $g(\varepsilon)$ [Eq. (B1)] in Eq. (44). Next, we discuss the EMA results in more detail.

B. EMA results

First, we analyze (within the EMA) the linewidth $\Gamma(\omega)$ in the phonon regime $\omega\ll\omega_{co}$. We limit the discussion to $p>p_c$ (the more physical situation). In the limit $\tau^{-1}=0$, we have[6] using Eqs. (70), (44), and (52),

$$\Gamma(\omega)\simeq\frac{\omega^{d+1}}{(p-p_c)^{d/2+1}}\sim\left[\frac{\omega}{\omega_{co}}\right]^d\omega_{co}^{d/2-1}\omega \tag{71}$$

($\Gamma\sim\omega^4$ in three dimensions), which is basically the Rayleigh-scattering[49,50] (of phonons from defects) result. At the phonon peak, we have $\omega=c_sq$, where $c_s\sim(p-p_c)^{1/2}$, so that the width is $\Gamma\sim q^{d+1}/(p-p_c)^{1/2}$; this is indeed the same result as for δ_q in Eq. (58) with $\tau^{-1}=0$. As τ^{-1} increases from zero, Eq. (71) is changed to

$$\Gamma(\omega)\simeq\frac{-\chi_d^{(2)}p_c(1-p_c)^{d/2}}{(p-p_c)^{d/2+1}}\omega^{d+1}+\left[\frac{2(1-p_c)p_cg(0)\omega^2}{(p-p_c)^2}+\frac{d\chi_d^{(1)}p_c(1-p_c)^{d/2}\omega^d}{(p-p_c)^{d/2+1}}\right]\tau^{-1} \ . \tag{72}$$

The first term is the same as Eq. (71) and is therefore a result of the spatial disorder, while the second term is the additional relaxation caused by dynamic fluctuations. For $d=3$ ($\chi_3^{(2)}=-\chi_3$, $\chi_3^{(1)}=0$), Eq. (72) reduces to

$$\Gamma(\omega)\simeq\frac{p_c(1-p_c)^{3/2}\chi_3}{(p-p_c)^{5/2}}\omega^4+\frac{2p_cg(0)(1-p_c)}{(p-p_c)^2}\omega^2\tau^{-1} \ . \tag{73}$$

The second term in Eq. (73) scales as $(\omega/\omega_{co})^2\tau^{-1}$. This term alone is consistent with the scaling assumption that $\Gamma(\omega)/\omega$ should be a function of ω/ω_{co} and $\tau\omega_{co}$ only. The first term, however, contradicts this assumption.[6] We shall define τ_{c1} as the τ for which $\Gamma(\omega)$ starts to change considerably from its value for $\tau^{-1}=0$. This will be when the second term in Eq. (73) or (72) becomes of the order of the first. Thus we find

$$\tau_{c1}\sim\left[\frac{\omega_{co}}{\omega}\right]^{d-1}\omega_{co}^{-d/2} \tag{74}$$

or $\tau_{c1}\sim(\omega_{co}/\omega)^2\omega_{co}^{-3/2}$ for $d=3$. Thus, unlike what is expected on general grounds, $\omega_{co}\tau_{c1}$ is not a function of ω/ω_{co} alone and (with ω/ω_{co} kept constant) increases as $\omega_{co}\to0$ (i.e., as $p-p_c\to0$). This is clearly related to the failure of scaling of the linewidth for $\tau^{-1}=0$. The second term in Eq. (73) implies, however, that for $\tau\ll\tau_{c1}$ (and for $d=3$), $\Gamma(\omega)/\omega$ does scale with τ and ω_{co}, at least to the first order in τ^{-1}. This *Ansatz* is checked numerically in Sec. IV C. We may define a second crossover value of

τ for which the position of the peak starts to change considerably (as τ^{-1} increases). This crossover can be easily obtained from the asymptotic expression for the sound velocity [Eq. (55)] to be at $\tau_{c2}\sim\omega_{co}^{-1}$, which is smaller than τ_{c1} (i.e., the peak broadens even before it starts to move).

For $\omega\gg\omega_{co}$ and $\tau^{-1}=0$, one finds[6] [from Eqs. (70), (44), and (52)] that the EMA linewidth obeys the Ioffe-Regel localization criterion[53,54] $\Gamma(\omega)\simeq\omega$, which is equivalent to the wavelength becoming of the order of the mean free path. Corrections to this result for small nonzero τ^{-1}, $\tau^{-1}\ll\omega_{co}$, are of order τ^{-1}/ω and therefore negligible for $\omega\gg\omega_{co}$. Thus, for $\omega\gg\omega_{co}$, the relaxation time marks the onset of localization, and relaxation caused by dynamic fluctuations is negligible in this limit.

It is of interest to obtain the linewidth in the large ω or τ^{-1} limit where the EMA becomes very accurate. Using for $\varepsilon\to\infty$, $g(\varepsilon)\simeq\varepsilon^{-1}-Z\varepsilon^{-2}$ [cf. Eq. (B4)] in Eq. (44), we find that, for $\omega,\tau^{-1}\gg1$,

$$\Gamma(\omega)\simeq\omega\frac{K''}{2K'}\simeq\frac{2(1-p)\omega^2\tau^3}{(1+\omega^2\tau^2)^2-2(1-p)(1-\omega^2\tau^2)\tau^2}\ . \tag{75}$$

This result is valid for all lattices in all dimensions. For $\tau\omega\ll1$ we have $\Gamma(\omega)\sim\omega^2\tau^3$ while for $\tau\omega\gg1$ it is $\Gamma(\omega)\sim\omega^{-2}\tau^{-1}$.

In Figs. 2–5 we present (within the EMA) the effect of increasing τ^{-1} on the dynamical structure factor $S(q,\omega)$, the linewidth $\Gamma(\omega)$, and the sound velocity $c_s(\omega)$ in a three-dimensional sc lattice ($p_c=\frac{1}{3}$) for $p-p_c\sim10^{-4}$ ($p=0.3334$). To obtain these results, we have solved Eq. (44) for the real and imaginary parts of the effective force constant $K(\omega)$ and used it in Eqs. (66), (69), and (70). We have used the expansion (51) for $g(\varepsilon)$ for $\tau\geq10^4$ and the exact expression [Eq. (B2)] (with $d=3$) for $g(\varepsilon)$ for $\tau\leq10^3$ [since the expansion (51) breaks down in this regime.]

Figures 2 and 3 show $S(q,\omega)$ multiplied by ω_{co}^2, against the reduced frequency ω/ω_{co} for different τ values. Figure 2(a) and 2(b) are for $q/q_{c0}=0.1$ and Fig. 3 is for $q/q_{c0}=10$. In Fig. 2(a) we see that, as τ^{-1} increases from zero, the phonon peak (the left peak) gets broadened and higher, while no change can be observed for the fracton peak (the peak on the right) on this plot. The change in the width becomes significant when $\tau\sim\tau_{c1}$ (e.g., $\tau_{c1}\sim10^6$ for $\omega\simeq\omega_{co}$ in Figs. 2 and 3). However, only when τ becomes larger than τ_{c1} by two orders of magnitude ($\tau\sim10^8$) are the results almost indistinguishable from those corresponding to the $\tau\to\infty$ limit. When τ approaches τ_{c2} ($\sim10^4$), the dip between the phonon and fracton peaks disappears completely and the presence of the fracton peak is hardly observed [Fig. 2(b)]. Also, for $\tau\leq\tau_{c2}$, the phonon peak starts to move to the right as τ^{-1} increases [Fig. 2(b)], a result of the fact that the

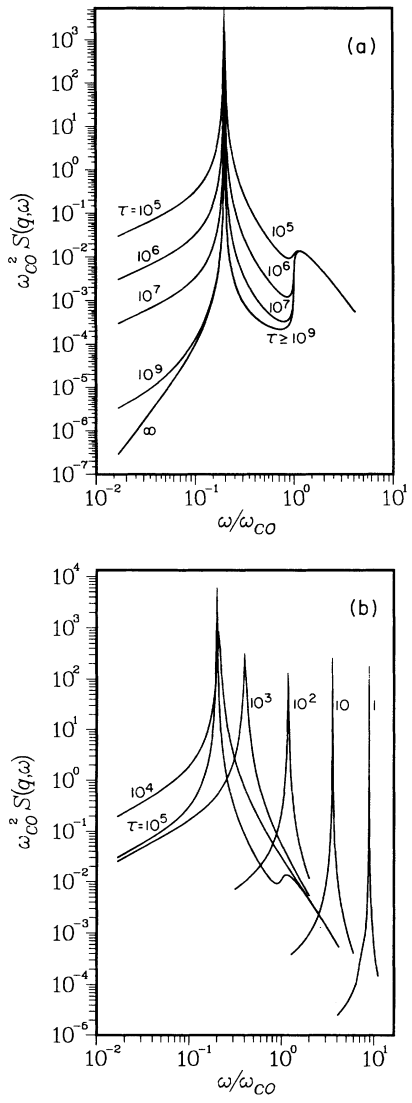

FIG. 2. Dynamical structure factor $S(q,\omega)$, multiplied by ω_{co}^2, vs the reduced frequency ω/ω_{co} for $q/q_{c0}=0.1$ and for different τ values. $(p-p_{c0})/(1-p_c)=10^{-4}$, $\omega_{co}=1.22\times10^{-4}$, and $q_{c0}=2.81\times10^{-2}$. (b) continues (a) for lower τ values.

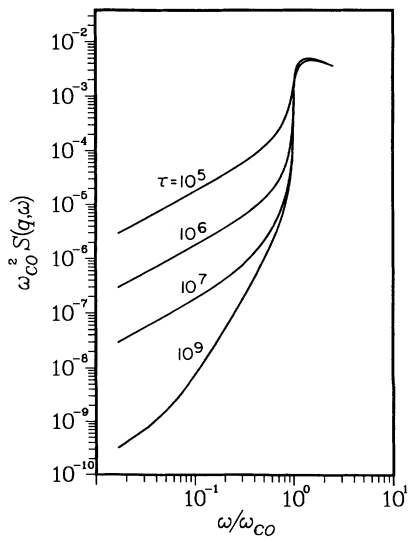

FIG. 3. Same as Fig. 2, but for $q/q_{c0}=10$.

sound velocity starts to change considerably. The width of the phonon peak also continues to grow after it starts to move. It goes through a maximum (when the phonon peak is somewhere between the static phonon and fracton peaks) and then starts narrowing for increasing τ^{-1}. Eventually, for $\tau \to 0$, it becomes a δ function situated at $\omega = \sqrt{p}\,q$ (i.e., $c_s = \sqrt{p}$). Note that even for small τ, the far right-hand side (RHS) of the phonon peak has the same shape; all lines for different τ values join together for $\omega \gg \omega_{co}$.

Figure 4 shows $\Gamma(\omega)/\omega$ plotted against the reduced frequency ω/ω_{co} on a log-log plot for a few values of τ. In the static limit $\tau = \infty$, the Rayleigh-scattering[6,49,50] behavior $\Gamma \sim \omega^4$ (slope 3 for the linear line) for $\omega \ll \omega_{co}$ and the Ioffe-Regel behavior[6,53,54] $\Gamma \sim \omega$ for $\omega \gg \omega_{co}$ can be clearly seen. For $\omega \ll \omega_{co}$ $\Gamma(\omega)$ increases with τ^{-1}. A significant change in $\Gamma(\omega)$ is seen only when $\tau \leq \tau_{c1}$ (for example, $\tau_{c1} \sim 10^8$ for $\omega = 0.1\omega_{co}$), as anticipated from Eq. (74). For $\omega \gg \omega_{co}$, $\Gamma(\omega)$ does not change significantly in the range of τ values plotted here, $10^5 \leq \tau \leq \infty$ [since it should start to change only when $\tau\omega \sim 1$; compare, e.g., with Fig. 6(a)]. For $\tau \ll \tau_{c1}$ the lines are again practically linear in the small-ω limit, with slope 1, as implied by the second term in Eq. (73); this is in contrast with the Rayleigh-scattering behavior of the $\tau = \infty$ line whose slope is 3.

Figure 5 shows the sound velocity $c_s(\omega)$ (divided by $\sqrt{\omega_{co}}$) plotted against ω/ω_{co} (on a log-log plot) for a few values of τ. For $\tau = \infty$, $c_s(\omega)$ does not depend on ω for $\omega \ll \omega_{co}$ and it crosses over to a $\omega^{1/2}$ behavior for $\omega \ll \omega_{co}$. The sharp dip seen at ω_{co} is a result of the sharp change in the EMA result for $K(\omega)$ at this frequency, as discussed following Eq. (47). As τ^{-1} is increased, $c_s(\omega)$ in the phonon (small-ω) regime starts to change when $\tau \sim \tau_{c2} \sim \omega_{co}$ ($\sim 10^4$ for $p = 0.3334$) behaves as $\sim \tau^{-1/2}$ for $\tau < 10^4$ and remains frequency independent. In the fracton regime ($\omega \gg \omega_c$), $c_s(\omega)$ does not depend

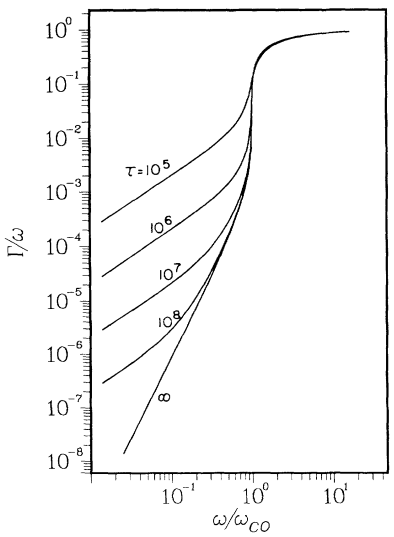

FIG. 4. $\Gamma(\omega)/\omega$ vs the reduced frequency ω/ω_{co} (on a log-log plot) for a few values of τ. $(p - p_c)/(1 - p_c) = 10^{-4}$ and $\omega_{co} = 1.22 \times 10^{-4}$.

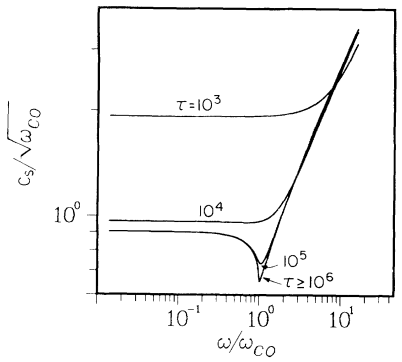

FIG. 5. Sound velocity $c_s(\omega)$, divided by $\omega_{co}^{1/2}$, plotted against the reduced frequency ω/ω_{co}, for a few values of τ. $(p - p_c)/(1 - p_c) = 10^{-4}$ and $\omega_{co} = 1.22 \times 10^{-4}$.

significantly on τ for $10^3 \leq \tau \leq \infty$, and its ω dependence becomes $\sim \omega^{1/2}$, as for the $\tau = \infty$ case. The crossover frequency ω_c shifts to higher frequencies, as seen from Eq. (49). The dip between the phonon and fracton regimes "smears out" and disappears as τ^{-1} is increased.

C. Scaling

1. *Scaling of the linewidth*

Following the scaling assumption[8] in the static case $\tau^{-1} = 0$, we now assume the following scaling behavior for the linewidth (where we expect scaling to hold only for $\tau^{-1}, \omega, \omega_{co} \ll 1$):

$$\Gamma(\omega) = \omega f_1(\omega/\omega_{co}, \tau\omega) , \tag{76}$$

where f_1 is the scaling function. The asymptotic behaviors of the linewidth may be derived using the Born approximation for scattering of phonons,[8,49,50]

$$\Gamma(\omega) \simeq |V|^2 N(\omega) , \tag{77}$$

where $N(\omega)$ is the density of states and V is the scattering matrix element. In the phonon regime ($\omega \ll \omega_{co}$) and the static limit ($\tau^{-1} = 0$), one then finds[8] $|V|^2 \sim \omega^2 \omega_{co}^{-\tilde{d}}$. Together with the scaled result for the phonon density of states,[7] $N_{ph}(\omega) \sim \omega_{co}^{\tilde{d}-d} \omega^{d-1}$, this leads to

$$\Gamma(\omega) \sim \omega^2 \omega_{co}^{-\tilde{d}} N_{ph}(\omega) \sim \omega_{co}^{-d} \omega^{d+1} . \tag{78}$$

If, however, $\tau\omega \ll \omega_{co}/\omega$ (still in the phonon regime), the relaxation is expected to be controlled by dynamic fluctuations. We may obtain the asymptotic behavior of $\Gamma(\omega)$ if we assume in addition that $|V|$ in Eq. (77) becomes independent of ω in this range of τ. Equation (76) and (77) then imply

$$\Gamma(\omega) \sim \omega_{co}^{\tilde{d}-d} \omega^{d-1} \tau^{-(2-\tilde{d})} , \tag{79}$$

which indeed reduces (for $d = 3$) to the EMA result (73) when $\tilde{d} = 1$, the EMA value for the fracton dimension.[5]

In Figs. 6(a) and 6(b), we see that the EMA results for the linewidth [Eqs. (44) and (70)] obey our scaling assumption [Eq. (76)] for $\tau < \tau_{c1}$ [where τ_{c1} is given by Eq.

(74)]. These results are obtained using the approximate expression Eq. (B3) for $g(\varepsilon)$ in Eq. (44) for practical reasons. In each figure $\Gamma(\omega)/\omega$ is plotted against the reduced frequency ω/ω_{co} for one value of $\tau\omega_{co}$ [$\sim\tau(p-p_c)$]: $\tau\omega_{co}\simeq 1$ and 10 in Figs. 6(a) and 6(b), respectively. Each value of $\tau\omega_{co}$ corresponds to a few values of ω_{co} and τ, giving the same product value. It is seen that, in this range of parameters, the EMA results satisfy our scaling assumption to a very good degree of accuracy. The scaling is better satisfied for $\omega \ll \omega_{co}$, in agreement with Eq. (74) (namely, τ_{c1} increases with decreasing ω, and therefore the condition $\tau \ll \tau_{c1}$ is better obeyed). Obviously, the choice for the τ values in these figures was in the range $\tau \ll \tau_{c1}$, and for $\tau \geq \tau_{c1}$ (including the $\tau=\infty$ case studied in Ref. 6) scaling is not obeyed.

2. Scaling of the sound velocity

Consider, first, the scaling of the frequency-dependent sound velocity in the static case. We assume that the sound velocity obeys the scaling law

$$c_s(\omega;p-p_c)=\omega^{\gamma} f_0(\omega/\omega_{co}) , \tag{80}$$

where the exponent γ is yet unknown. Since c_s is independent of ω for $\omega \ll \omega_{co}$, the scaling function f_0 must behave as $f_0(x)\sim x^{-\gamma}$ for $x \ll 1$. In order to satisfy $c_s \simeq \omega_{co}^{\theta/(2+\theta)}$, we must choose

$$\gamma=\frac{\theta}{2+\theta} . \tag{81}$$

For $\omega \gg \omega_{co}$, c_s should be independent of ω_{co}. Therefore, for $x \gg 1$, we must have $f_0(x)\rightarrow$const and $c_s \sim \omega^{\gamma}$ in this limit. In the EMA, $\theta=2$ and $\gamma=\frac{1}{2}$.

Turning now to the dynamic case, we assume a scaling law of the form

$$c_s(\omega,\tau;p-p_c)=\omega^{\gamma} f_2(\omega/\omega_{co},\tau\omega) . \tag{82}$$

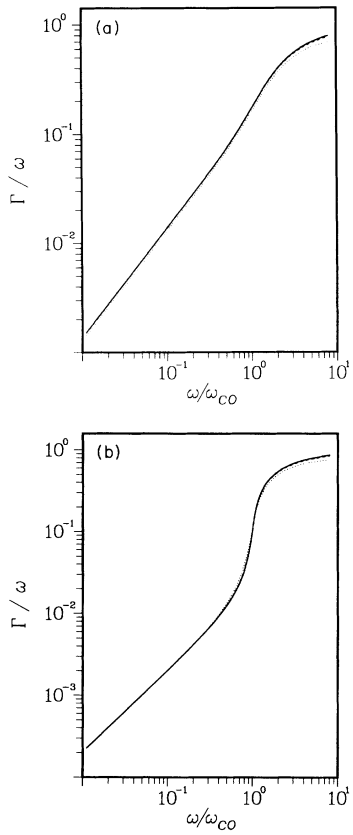

FIG. 6. $\Gamma(\omega)/\omega$ (the linewidth divided by frequency) against the reduced frequency ω/ω_{co} for one value of $\tau\omega_{co}$, $\tau(p-p_c)/(1-p_c)=1$ and 10 in (a) and (b), respectively (using different τ and p). The results were obtained by solving Eq. (44), using the approximate Eq. (B3) for $g(\varepsilon)$, and Eq. (70) for $\Gamma(\omega)$. (a) Solid line, $p=0.3334$, $\tau=10^4$; dashed line, $p=0.334$, $\tau=10^3$; dotted line, $p=0.34$, $\tau=100$. (b) Solid line, $p=0.333\,34$, $\tau=10^6$ and $p=0.3334$, $\tau=10^5$; dotted line, $p=0.334$, $\tau=10^4$.

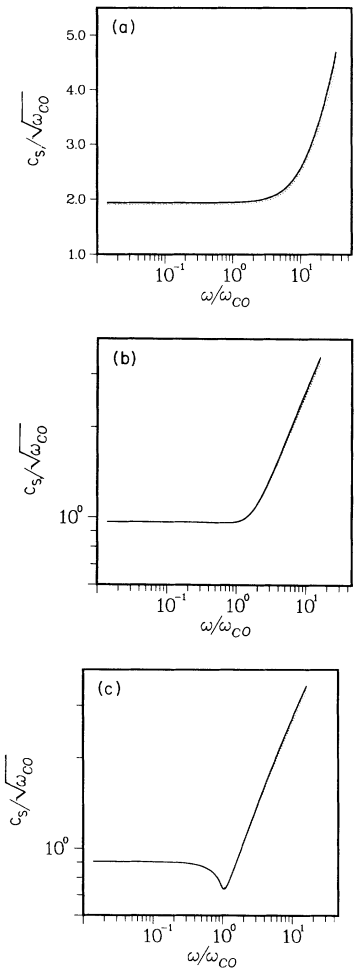

FIG. 7. Sound velocity $c_s(\omega)$, normalized by $\omega_{co}^{-1/2}$, vs ω/ω_{co} for a few values of $\tau\omega_{co}$, $\tau(p-p_c)/(1-p_c)=0.1$, 1, and 10 in (a), (b), and (c), respectively (using different τ and p). The results were obtained by solving Eq. (44), using Eq. (B3) for $g(\varepsilon)$, and Eq. (69) for $c_s(\omega)$. (a) Solid line, $p=0.333\,34$, $\tau=10^4$; dashed line (almost coincident with the solid line), $p=0.3334$, $\tau=10^3$; dotted line, $p=0.334$, $\tau=10^2$. (b) Solid line, $p=0.333\,34$, $\tau=10^5$ and $p=0.3334$, $\tau=10^4$; dotted line, $p=0.334$, $\tau=10^3$. (c) Solid line, $p=0.333\,34$, $\tau=10^6$ and $p=0.3334$, $\tau=10^5$; dotted line, $p=0.334$, $\tau=10^4$.

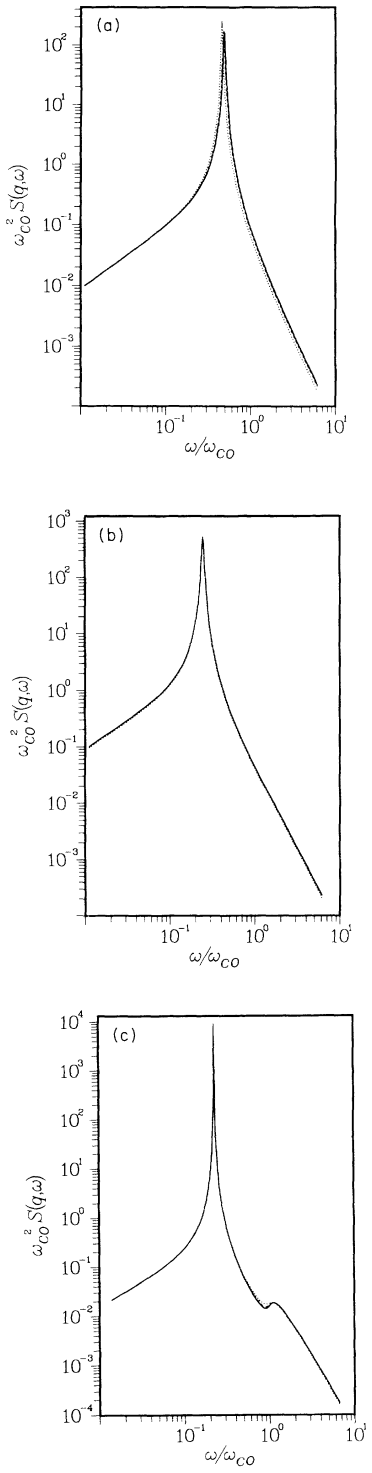

FIG. 8. Dynamical structure factor $S(q,\omega)$, multiplied by ω_{co}^2, vs the reduced frequency ω/ω_{co} for $q/q_{c0}=0.1$ and for a few values of $\tau\omega_{co}$, $\tau(p-p_c)/(1-p_c)=0.1$, 1, and 10 in (a), (b), and (c), respectively (using a few values of τ and p). (a) Solid line, $p=0.3334$, $\tau=10^3$; dashed line (almost coincident with the solid line), $p=0.334$, $\tau=10^2$; dotted line, $p=0.34$, $\tau=10$. (b) Solid line, $p=0.3334$, $\tau=10^4$ and $p=0.334$, $\tau=10^3$; dotted line, $p=0.34$, $\tau=10^2$. (c) Solid line, $p=0.3334$, $\tau=10^5$; dashed line (almost coincident with the solid line), $p=0.334$, $\tau=10^4$; dotted line, $p=0.34$, $\tau=10^3$.

In Figs. 7(a)–7(c), we check whether the EMA results [Eqs. (69) and (44) with Eq. (B3) for $g(\varepsilon)$] obey the scaling assumption Eq. (80). We plot the sound velocity, normalized by $\omega_{co}^{-1/2}$, against ω/ω_{co} for a few values of $\tau\omega_{co}$ [$\tau\omega_{co}\simeq 0.1$, 1, and 10 in Figs. 7(a), 7(b), and 7(c), respectively] where in each plot we use a few values of τ and ω_{co} that give the same $\tau\omega_{co}$. It is seen that the EMA results obey the scaling assumption for the sound velocity to a very good degree of accuracy in this range of τ. Deviations from scaling exist mainly for $\omega \gg \omega_{co}$. For $\tau \gg \tau_{c1}$ [which is not the case in Figs. 7(a)–7(c)], we have found that deviations from scaling exist also in the vicinity of ω_{co}. This is consistent with the results for the static case, $\tau=\infty$, studied in Ref. 6.

3. *Scaling of the dynamical structure factor*

The scaling assumptions for the linewidth and sound velocity [Eqs. (76) and (80)] can be combined in the general expression for the dynamical structure factor [Eqs. (67) and (68)] in order to obtain the scaling form of this quantity. In addition, we suggest scaling of the dynamical structure factor with q/q_{c0}. Using the fact that $q_{c0}\sim\xi^{-1}\sim\omega_{co}^{2/(2+\theta)}$ (ξ is the percolation correlation length), we get [with $\gamma=\theta/(2+\theta)$]

$$\omega^{\gamma-1}q_{c0}=A\left[\frac{\omega_{co}}{\omega}\right]^{2/(2+\theta)}, \tag{83}$$

where A is a numerical constant. This leads to the scaling law

$$S(q,\omega,\tau;p-p_c)=\omega^{-2}\Psi(q/q_{c0},\omega/\omega_{co},\tau\omega)\ , \tag{84}$$

where Ψ is the scaling function.

In Figs. 8(a)–8(c) we check our scaling assumption [Eq. (84)] for several values of $p-p_c$ and for $\tau<\tau_{c1}$. Since the EMA results for both $\Gamma(\omega)$ and $c_s(\omega)$ were found to obey our scaling assumptions (for τ in this range), it is clear that $S(q,\omega)$ also obeys scaling. We plot $\omega_{co}^2 S(q,\omega)$ as a function of ω/ω_{co}, keeping q/q_{co} and $\tau\omega_{co}$

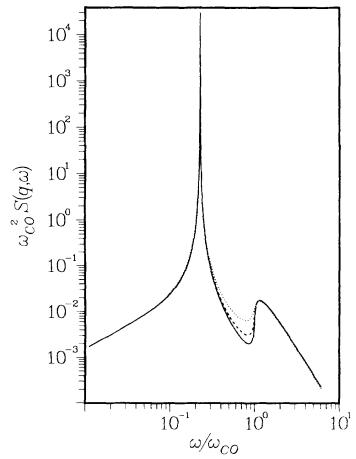

FIG. 9. Same as Fig. 8, but for $\tau(p-p_c)/(1-p_c)=100$. Solid line, $p=0.3334$, $\tau=10^6$; dashed line, $p=0.334$, $\tau=10^5$; dotted line, $p=0.34$, $\tau=10^4$.

constant [$q/q_{co}=0.1$ and $\tau\omega_{co}\simeq 0.1$, 1, and 10 in Figs. 8(a), 8(b), and 8(c), respectively], while for each plot we used a few values of τ and p that give the same $\tau\omega_{co}$. The accuracy of scaling exhibited by the EMA is striking. It is better for $\tau \ll \tau_{c1}$ than for $\tau \sim \tau_{c1}$ as was anticipated analytically, although for τ too small scaling is also not obeyed very well [Fig. 5(a)]. For comparison we also show, in Fig. 9, the results for $\tau\omega_{co}\simeq 100$, where it is seen that scaling is not obeyed at the dip in the vicinity of ω_{co}, similar to the $\tau=\infty$ case seen in Fig. 1 of Ref. 6.

There were a few speculations[4-8] concerning the failure of the EMA results to scale with a single frequency ω_{co} in the static ($\tau^{-1}=0$) limit of the present model. They invoke either the approximation made in the EMA or the possibility of another crossover frequency ω_{IR} for the crossover to Ioffe-Regel behavior $\Gamma(\omega)\sim\omega$. The fact that for $\tau^{-1}>0$ scaling is obeyed to a good accuracy for a large range of parameter values suggests that in these cases the EMA is quite reliable, even if it is less accurate in the static case. Recent simulations[11] (for static networks) indeed show that there is no hump in the density of states $N(\omega)$ near ω_{co}, implying that the hump seen in the dynamic structure factor is also an artifact of the EMA. (Rather, a hump appears at the fracton Debye frequency.) Yet, for the range of τ values where our scaling assumption is obeyed, the EMA dynamical structure factor does not show such a hump. Therefore these simulations do not contradict our results.

V. EXPERIMENTAL IMPLICATIONS

The theory advanced here simply recovers the EMA results[4-6] for the static bond percolation systems ($\tau^{-1}=0$). It is therefore consistent with specific-heat and thermal-conductivity measurements below the glass transition[2,3,12,19,22] (see Sec. I), since τ is expected to be practically infinite well below T_g. Our theory then deals with the behavior of these and other observables as the temperature is raised above T_g to form a liquid. To make this theory useful, it is essential to estimate the temperature dependence of the model parameters.

For glass-forming polymers, we can gain some insight by noting that a single polymer chain forms a fractal object[26] (for distances much larger than the persistance length), and if no forces are acting on it by the environment, its fracton dimension is always $\tilde{d}=1$ (irrelevant of its fractal dimension or dimensionality of the embedding space).[1] Consequently, we may assume as an *Ansatz* that, in the absence of cross-links, the fractal correlation length ξ (for the force constants) scales with the density just as the polymer correlation length[26] ξ_p (the mesh size of the network) that appears in the theory of polymer melts.[55] In cross-linked polymer networks (with either transient or permanent cross-links), the distance between cross-links may also serve as an estimate of the correlation length. For example, in solvent-free polymer electrolytes,[25,56] the number of ions and, hence, the number of transient cross-links (per unit chain) formed by the doped ions are both known, and the reduction of the correlation length can be estimated. Alternatively, at low temperatures it is possible to estimate the correlation length directly from specific-heat and thermal-conductivity measurements.[12] For example, in epoxy resin[12] these measurements suggest that $\xi\simeq 100$ Å.

A well-accepted model of semidilute polymer solutions is that of an array of densely packed "blobs" of linear size ξ_p, the (monomer) density correlation length. Each blob consists of a self-avoiding (or Gaussian) chain, which (in the present context) is a fractal object. Thus various properties of semidilute solutions obey simple scaling laws governed by ξ_p. This could have made such systems natural for application of the phonon-fracton model. However, since the polymer is surrounded by solvent molecules, the force matrix is rather uniform in space. Although the solvent is absent in polymer melts, scaling theory usually breaks down at such high densities.[26] In semidilute polymer solutions,[26] ξ_p scales with the monomer number density ρ as $\xi_p\sim\rho^{-3/4}$, while in polymer melts ξ_p is much smaller than the former and the scaling exponent is $\frac{1}{2}$ rather than $\frac{3}{4}$ (namely, $\xi_p\sim\rho^{-1/2}$).[57]

Consider now a (pure) glass-forming polymer melt. In view of the above discussion, we assume[55] as an *Ansatz* that the fractal linear size ξ (associated with the force constants) continues to scale with the density as ξ_p of the *semidilute solutions*, namely, $\xi_p\sim\rho^{-3/4}$. On the other hand, for a percolation network, $\xi\sim(p-p_c)^{-\nu}$ (where, e.g., $\nu=\frac{1}{2}$ in the EMA). Equating the two lengths, we find $p-p_c\sim\rho^{3/(4\nu)}$, a result which maps the (static) percolation model onto the glassy melt. Similarly, since in the phonon-fracton model $\omega_{co}\sim\xi^{-(1+\theta/2)}$, $q_{c0}\sim\xi^{-1}$ and (in the static $\tau^{-1}=0$ case) $c_s\sim\xi^{-\theta/2}$, we find $\omega_{co}\sim\rho^{3/4(1+\theta/2)}$, $q_{c0}\sim\rho^{3/4}$ and (for $T<T_g$) $c_s\sim\rho^{3\theta/8}$. Since[1] $\tilde{d}=1$ and[26] $\bar{d}=\frac{5}{3}$ for swollen linear polymers, we have $\theta=2(\bar{d}/\tilde{d}-1)=\frac{4}{3}$. This yields $\omega_{co}\sim\rho^{5/4}$ and $c_s\sim\rho^{1/2}$. This result for c_s should be valid well below T_g. As T is raised above T_g, we expect that τ^{-1} would start to increase (from zero), but the relation $c_s\sim\rho^{1/2}$ will still approximately hold until $\tau\omega_{co}\sim\tau\rho^{5/4}\sim 1$. The temperature at which this occurs we denote T^* ($>T_g$). Then, according to Eq. (55), larger dynamic fluctuations will cancel some of the decrease in the density. These predictions are consistent with experimental observations: Below T_g, *both* the density and sound velocity show a slow decrease with temperature.[58,59] Just above T_g, *both* show a more rapid decrease with temperature;[58] however, while the density continues to drop with T, the sound velocity flattens at some T^*, just as stated above.[28,60] In spite of this consistency, we note that Eq. (56) does pose a severe problem for the present model, as it implies an increase of c_s with temperature for $T>T^*$.

Consider now a (solvent-free) polymer-electrolyte network [e.g., poly(propylene oxide) or poly(ethylene oxide)]. When the network is doped with salt, the Lewis-base atoms (oxygen, nitrogen, etc.) usually form a quasi-tetrahedral configuration around the alkali ions, whereas the anions are relatively free and their contribution to transient cross-links can be neglected.[28,54] Let N_{c0} be the number of monomers between two consecutive (transient) cross-links along a chain, in an ionic-free network. In a doped network with a given ratio $N_{O:M}$ of monomers to metal ions, for every N_{c0} monomers on a single chain

there are (on the average) about $1+(N_{c0}/N_{O:M})$ "contact points" to other chains. This means that $N_c \simeq N_{c0}/[1+(N_{c0}/N_{O:M})]$ is the mean number of monomers along a chain between two consecutive "cross-links." One can use[26] $N_{c0} \sim \xi_f^{5/3} \sim \rho^{-5/4}$, where ξ_f is the correlation length of an ionic-free network, as discussed above. To obtain the fractal size, we can use[26] $\xi \sim N_c^{3/5}$. Thus, for $T < T_g$, we have $c_s \sim N_c^{-3\theta/10}$ or (using $\theta = \frac{4}{3}$)

$$c_s \sim (A\rho^{5/4} + 1/N_{O:M})^{2/5} , \tag{85}$$

where A is a numerical constant. Thus c_s increases with decreasing $N_{O:M}$, as experimentally observed.[28] Similarly $\omega_{co} \sim A\rho^{5/4} + 1/N_{O:M}$ and $q_{c0} \sim [A\rho^{5/4} + 1/N_{O:M}]^{3/5}$.

Consider now the density dependence of the linewidth Γ of the phonon peak. Below T_g the phonon-fracton theory predicts the Rayleigh-scattering behavior $\Gamma \sim q^4$. Just above T_g we predict $\Gamma \sim q^2$ (assuming $\xi^{\theta/2} q^2 \ll \tau^{-1}$), which is similar to the prediction of Mountain theory[32-34] and is experimentally well confirmed. Using again the estimates for the correlation length in polymeric glasses and the scaling results for Γ [Eqs. (78) and (79)], we find, for pure polymers,

$$\Gamma \sim \rho^{-7/4} q^4, \quad T \ll T_g , \tag{86}$$

$$\Gamma \sim \rho^{-3/2} \tau^{-1} q^2, \quad T > T_g . \tag{87}$$

As τ should decrease rapidly with temperature just above T_g, Eq. (87) indeed explains why the phonon peak shows substantial broadening when one crosses from the glass to the liquid phase. For a complexed polymer electrolyte, we similarly find $\Gamma \sim N_c^{7/5} q^4$ (for $T \ll T_g$) and $\Gamma \sim N_c^{6/5} \tau^{-1} q^2$ (for $T > T_g$). It should be easy to check these predictions experimentally.

To conclude this section, we would like to stress a few points: (i) In Sec. IV B it was noted that as τ^{-1} increases from zero (keeping p fixed), the width of the phonon peak increases, passes through a maximum, and then diminish again. Since τ should decrease monotonously (and rapidly) with increasing temperature above the glass transition, a similar behavior is expected for increasing temperature. This is indeed the *universal* behavior observed in liquids above their glass transition.[28] However, Mountain phenomenological theory[32-34] offers another explanation for this effect. (ii) As seen in Fig. 2(a), the "background" line on the LHS of the phonon peak is very low for $\tau = \infty$ and increases substantially as τ^{-1} increases from zero, while a much more moderate effect is observed on the RHS to the peak (i.e., the peak is not broadened uniformly). This is consistent with experimental observations below and above the glass transition.[58] Another explanation for this effect is offered by a phenomenological "Mountain-like" theory.[58] (iii) Although the actual temperature dependence of the model parameter τ is not known, we expect it to have the Vogel-Tamman-Fulcher[61] form, $\tau = \tau_0 \exp[B/(T - T_0)]$, where T_0 is an "ideal" (or "equilibrium") glass transition temperature and where B and τ_0 are constants. (iv) τ can also be obtained *independently* from the same Brillouin experiment by extracting the monomer diffusion coefficient from the width of the quasielastic Brillouin line and deducing the monomer diffusion time over a monomer size. (v) The temperature T^*, which is defined above as the temperature at which the sound velocity shows no more substantial decrease with increasing temperature, seems to be closely related to the kinetic glass transition temperature T_c which appears in mode-coupling theories.[62]

Finally, we note that the ideas presented in this section are somewhat *speculative* in nature and cannot be regarded as the final word on this issue. However, a similar approach to the one presented here has recently been successful in analyzing the Raman spectrum of amorphous polymers.[27]

VI. CONCLUSIONS

In this paper we have generalized (within the EMA) the Alexander-Orbach theory for phonon-fracton behavior to time-dependent percolating networks. Our formalism yields a general procedure for obtaining the frequency-dependent effective force constant $K(\omega)$ [cf. Eqs. (40)–(43)] and shows that, just as for the frequency-dependent diffusion coefficient, $K(\omega)$ depends on ω and on the network relaxation times τ_j (only) through combinations of the form $\omega - i/\tau_j$. For situations where the dynamics is associated with a single relaxation time, this leads to the analytic continuation rule Eq. (46), similar to that found for diffusion.

Knowledge of the effective force constant makes it possible to calculate any physical observable of interest through the Green's-function formalism. In this work we have focused attention on the dispersion relation (Sec. III) and the dynamical structure factor (Sec. IV). For the latter quantity, dynamic fluctuations in the disorder have a significant effect. First, the phonon peak is broadened as the fluctuation process is switched on, namely, as τ^{-1} increases from zero. This extra broadening is negligible until $\tau \sim \tau_{c1}$ is reached [Eq. (74)]. As the fluctuations become faster, the width goes through a maximum and then diminishes again (the "motional narrowing" effect of Kubo line-shape theory[63]). The sound velocity increases monotonously with τ^{-1}; this increase is negligible until $\tau \sim \tau_{c2} \sim \omega_{co}^{-1}$ is reached.

In order to relate to experiment, the temperature dependence of the model parameters has to be set. A way to circumvent this difficulty is provided in Sec. V by equating the percolation correlation length with the polymer correlation length for screening of the excluded volume interaction. Decrease of the sound velocity with temperature is explained via volume expansion of the material. We note that the Mountain relaxation theory[32-34] suggests an alternative explanation for this effect. However, Mountain theory predicts that the linewidth should be proportional to q^2 below the glass transition (infinite relaxation time), just as for a Navier-Stokes liquid, while the present model leads to a q^4 behavior (Rayleigh's law) which is more likely to be correct.

Obviously, calculation of other observables can help to support our model, for example, calculation of the specific heat, which involves only one new input, the density of states. The latter can be readily obtained from the Green's function. The specific heat increases significantly

when passing from below to above the glass transition,[64] and it would be interesting to see how the present model predicts this change.

ACKNOWLEDGMENTS

Most of this work was carried out at Tel-Aviv University. I am grateful to Professor Abraham Nitzan for suggesting this topic and for guidance and many useful discussions. I am also indebted to J. Klafter, M. Bixon, S. Alexander, O. Entin-Wohlman, M. Feingold, M. E. Cates, M. A. Ratner, L. M. Torell, M. Pietralla, and J. K. Kruger for stimulating discussions. This work was supported in part by EC Grant No. SC1 0288-C.

APPENDIX A: FORMAL SOLUTION FOR EQS. (28)

Here we obtain Eq. (30) from Eqs. (28). Taking the Laplace transform $\mathbf{A}(\vec{\sigma},z)=\int_0^\infty dt\, e^{-zt}\mathbf{A}(\vec{\sigma},t)$ of Eqs. (28), we get

$$z\mathbf{P}(\vec{\sigma},z)-\mathbf{P}_0\rho(\vec{\sigma})=-\mathbf{W}\cdot\mathbf{U}(\vec{\sigma},z)+\hat{\Omega}\mathbf{P}(\vec{\sigma},z)\ , \tag{A1a}$$

$$z\mathbf{U}(\vec{\sigma},z)-\mathbf{U}_0\rho(\vec{\sigma})=\mathbf{P}(\vec{\sigma},z)+\hat{\Omega}\mathbf{U}(\vec{\sigma},z)\ . \tag{A1b}$$

In order to keep the order of noncommuting quantities, we invert Eqs. (A1) step by step. By definition, $\hat{\Omega}\rho(\vec{\sigma})=0$ [cf. Eq. (19)], and thus

$$(z-\hat{\Omega})^{-1}\rho(\vec{\sigma})=z^{-1}\rho(\vec{\sigma})\ , \tag{A2}$$

whence, from Eq. (A1b),

$$\mathbf{U}(\vec{\sigma},z)=(z-\hat{\Omega})^{-1}\mathbf{P}(\vec{\sigma},z)+z^{-1}\mathbf{U}_0\rho(\vec{\sigma})\ . \tag{A3}$$

Substituting Eq. (A3) into Eq. (A1a) and solving for $\mathbf{P}(\vec{\sigma},z)$, we get

$$\mathbf{P}(\vec{\sigma},z)=\mathbf{g}_{pp}(\vec{\sigma},z)\cdot\mathbf{P}_0+\mathbf{g}_{pu}(\vec{\sigma},z)\cdot\mathbf{U}_0\ , \tag{A4}$$

where the partially averaged Green's operators $\mathbf{g}_{pp}(\vec{\sigma},z)$ and $\mathbf{g}_{pu}(\vec{\sigma},z)$ are formally given by

$$\mathbf{g}_{pp}(\vec{\sigma},z)=[(z-\hat{\Omega})\mathbf{1}+\mathbf{W}(z-\hat{\Omega})^{-1}]^{-1}\rho(\vec{\sigma})\ , \tag{A5a}$$

$$\mathbf{g}_{pu}(\vec{\sigma},z)=-z^{-1}[(z-\hat{\Omega})\mathbf{1}+\mathbf{W}(z-\hat{\Omega})^{-1}]^{-1}\cdot\mathbf{W}\rho(\vec{\sigma})\ . \tag{A5b}$$

Using again $\hat{\Omega}\rho(\vec{\sigma})=0$, $\mathbf{g}_{pp}(\vec{\sigma},z)$ can be simplified to

$$\mathbf{g}_{pp}(\vec{\sigma},z)=z[(z-\hat{\Omega})^2\mathbf{1}+\mathbf{W}]^{-1}\rho(\vec{\sigma})\ . \tag{A6}$$

In addition, $\mathbf{g}_{pp}(\vec{\sigma},z)$ and $\mathbf{g}_{pu}(\vec{\sigma},z)$ can be simply related to each other. To find this relation, we rewrite $\mathbf{g}_{pu}$ as

$$\begin{aligned}\mathbf{g}_{pu}(\vec{\sigma},z)&=-z^{-1}(z-\hat{\Omega})[(z-\hat{\Omega})^3\mathbf{1}+(z-\hat{\Omega})\mathbf{W}]^{-1}\cdot(z-\hat{\Omega})\mathbf{W}\rho(\vec{\sigma})\\&=-z^{-1}(z-\hat{\Omega})[(z-\hat{\Omega})^3\mathbf{1}+(z-\hat{\Omega})\mathbf{W}]^{-1}\cdot[(z-\hat{\Omega})^3\mathbf{1}+(z-\hat{\Omega})\mathbf{W}-(z-\hat{\Omega})^3\mathbf{1}]\rho(\vec{\sigma})\\&=-z^{-1}(z-\hat{\Omega})\{\mathbf{1}-[(z-\hat{\Omega})^3\mathbf{1}+(z-\hat{\Omega})\mathbf{W}]^{-1}(z-\hat{\Omega})^3\}\rho(\vec{\sigma})\\&=-z^{-1}\{z\mathbf{1}-z^3[(z-\hat{\Omega})^2\mathbf{1}+\mathbf{W}]^{-1}\}\rho(\vec{\sigma})\ ,\end{aligned} \tag{A7}$$

where we have again used $\hat{\Omega}\rho(\vec{\sigma})=0$. Thus

$$\mathbf{g}_{pu}(\vec{\sigma},z)=-\rho(\vec{\sigma})\mathbf{1}+z\mathbf{g}_{pp}(\vec{\sigma},z)\ . \tag{A8}$$

$\mathbf{U}(\vec{\sigma},z)$ can be now found by substituting $\mathbf{P}(\vec{\sigma},z)$ in Eq. (A3) [using again Eq. (A2)]. This leads to Eq. (30).

APPENDIX B

Expressions for the lattice Green's function of the origin $g(\varepsilon)$ are summarized here. In d dimensions it is generally given by[44,40]

$$g(\varepsilon)=\frac{1}{(2\pi)^d}\int_{\mathrm{BZ}}d\mathbf{q}\left[\varepsilon+\sum_{\mathbf{a}}(1-e^{i\mathbf{q}\cdot\mathbf{a}})\right]^{-1}\ , \tag{B1}$$

where $\mathbf{a}$ are vectors directing from an origin to the nearest-neighbor sites, and the integral is carried over the first Brillouin zone. For a simple cubic lattice (in d dimensions), Eq. (B1) can be transformed to[43]

$$g(\varepsilon)=\tfrac{1}{2}\int_0^\infty dt\,\exp[-(d+\tfrac{1}{2}\varepsilon)t][I_0(t)]^d\ , \tag{B2}$$

where $I_0(t)$ is the modified Bessel function of order zero. A useful approximate expression for a 3D simple cubic lattice has been obtained by Odagaki and Lax:[40]

$$g(\varepsilon)=2\{\varepsilon+6+[\varepsilon(\varepsilon+12)]^{1/2}\}^{-1}\ . \tag{B3}$$

$g(\varepsilon)$ is also the Laplace transform of the random walker probability for returning to the origin at time t, $P_0(t)$.[1] Using, for small t, $P_0(t)\simeq 1-Zt+o(t^2)$, where Z is the coordination number, one obtains, for large ε,

$$g(\varepsilon)\simeq\varepsilon^{-1}-Z\varepsilon^{-2}+o(\varepsilon^{-3})\ , \tag{B4}$$

which is valid for an arbitrary lattice (in all dimensions).

APPENDIX C

Here we obtain Eq. (59) in the common way. We write the results directly for the scalar elasticity model, where the different components of the displacement vector are not correlated (in Sec. II we treated the dynamics of a single component). Consider a specific realization of the dynamically disordered system denoted by the bond configuration vector $\vec{\sigma}(t)$. For any such realization, the intensity of the scattered light is given by[44,45]

$$\frac{d^2\sigma_1}{d\Omega\,dE}=\frac{N}{\hbar}S_1(\mathbf{q},\omega)\ , \tag{C1}$$

$$S_1(\mathbf{q},\omega)=e^{-2W}\frac{q^2}{2\pi N}\int_{-\infty}^{\infty}dt\,e^{i\omega t}\sum_{i,j}e^{-i\mathbf{q}\cdot\mathbf{R}_{ij}}\langle U_i(0)U_j(t)\rangle_T\ . \tag{C2}$$

Here W is the Debye-Waller factor $2W=q^2\langle U(0)^2\rangle_T$ and $\mathbf{R}_{ij}=\mathbf{R}_j-\mathbf{R}_i$ is the vector separation between sites i and j. The angular brackets denote thermal average. The (standard) next step is to argue that by summing over all scattering atoms located at sites i in Eq. (C2) we pick up all realizations of the system (with respect to both the spatial disorder and stochastic dynamics of the bonds) and so this is approximately equivalent to (N times) the ensemble average over all realizations of the system (namely, all realizations of the initial condition for the bond configuration and all realizations of paths for each initial condition) with a fixed site index i. Equation (C2) is then rewritten as

$$S_1(\mathbf{q},\omega)=e^{-2W}\frac{q^2}{2\pi}\int_{-\infty}^{\infty}dt\,e^{i\omega t}\sum_{j}e^{-i\mathbf{q}\cdot\mathbf{R}_{ij}}\langle\langle U_i(0)U_j(t)\rangle_T\rangle\ , \tag{C3}$$

where the second angular brackets denote such an ensemble average. The thermal and ensemble averages can now be interchanged. This can be seen from the form of Eq. (32) showing that the calculation of $\langle\langle U_i(0)U_j(t)\rangle_T\rangle$ involves the fully averaged Green's functions $g_{ij}(t)$ and equilibrium correlation functions of the form $\langle U_i(0)U_k(0)\rangle_T$ and $\langle U_i(0)P_k(0)\rangle_T$. We avoid the explicit calculation, and we now make use of standard results. In the theory of lattice dynamics, it is shown that[44]

$$\int_{-\infty}^{\infty}dt\,e^{i\omega t}\langle U_i(0)U_j(t)\rangle_T=2\hbar[n(\omega)+1]\mathrm{Im}G_{ij}(\omega-i0)\ , \tag{C4}$$

where $n(\omega)$ is the Bose population factor,

$$n(\omega)=(e^{\beta\hbar\omega}-1)^{-1}\ , \tag{C5}$$

with $\beta=1/k_BT$ and where $G_{ij}(\omega)$ is the Green's function of the system [$G_{ij}(\omega-i0)$ is the advanced Green's function]. $G_{ij}(\omega)$ is now identified with an element (in Laplace space) of the fully averaged Green's operator $g_{ij}(z)$ of the theory of Sec. II [Eqs. (33) and (34)],

$$G_{ij}(\omega-i0)=-g_{ij}(i\omega+0)\equiv-\langle i|\mathbf{g}(i\omega+0)|j\rangle\ . \tag{C6}$$

This leads to Eq. (59).

---

*Present address: Department of Chemistry, University of California, LA, CA 90024-156905.

[1]S. Alexander and R. Orbach, J. Phys. (Paris) Lett. **43**, 1625 (1982).
[2]S. Alexander, C. Laermans, R. Orbach, and H. M. Resenberg, Phys. Rev. B **28**, 4615 (1983).
[3]P. F. Tua, S. J. Putterman, and R. Orbach, Phys. Lett. **98A**, 357 (1983).
[4]O. Entin-Wohlman, S. Alexander, R. Orbach, and Kin-Wah Yu, Phys. Rev. B **29**, 4588 (1984).
[5]B. Derrida, R. Orbach, and Kin-Wah Yu, Phys. Rev. B **29**, 6645 (1984).
[6]G. Polatsek and O. Entin-Wohlman, Phys. Rev. B **37**, 7726 (1988).
[7]A. Aharony, S. Alexander, O. Entin-Wohlman, and R. Orbach, Phys. Rev. B **31**, 2565 (1985).
[8]A. Aharony, S. Alexander, O. Entin-Wohlman, and R. Orbach, Phys. Rev. Lett. **58**, 132 (1986).
[9]S. Alexander, Physica **140A**, 397 (1986).
[10]S. Alexander, Phys. Rev. B **40**, 7953 (1989).
[11]K. Yakubo and T. Nakayama, Phys. Rev. B **40**, 517 (1989); T. Nakayama, in *Phonons 89*, edited by W. Ludwig, S. Hunklinger, and G. Weiss (World Scientific, Singapore, 1989), p. 646.
[12]S. Kelham and H. M. Rosenberg, J. Phys. C **14**, 1737 (1981).
[13]E. Courtens, J. Pelous, J. Phalippou, R. Vacher, and T. Woignier, Phys. Rev. Lett. **58**, 128 (1987).
[14]R. Vacher, T. Woignier, J. Pelous, and E. Courtens, Phys. Rev. B **37**, 6500 (1988).
[15]E. Courtens and R. Vacher, Z. Phys. B **68**, 355 (1987).
[16]Y. Tsujimi, E. Courtens, J. Pelous, and R. Vacher, Phys. Rev. Lett. **60**, 2757 (1988); R. Vacher, T. Woignier, J. Pelous, G. Coddens, and E. Courtens, Europhys. Lett. **8**, 161 (1989); R. Vacher, E. Courtens, G. Coddens, J. Pelous, and T. Woignier, Phys. Rev. B **39**, 7384 (1989).
[17]E. Courtens, R. Vacher, J. Pelous, and T. Woignier, Europhys. Lett. **6**, 245 (1988).
[18]M. Arai and J. E. Jorgensen, Phys. Lett. A **133**, 70 (1988).
[19]S. Alexander, O. Entin-Wohlman, and R. Orbach, Phys. Rev. B **34**, 2726 (1986).
[20]S. Alexander, O. Entin-Wohlman, and R. Orbach, Phys. Rev. B **32**, 6447 (1985).
[21](a) D. Stauffer, Phys. Rep. **54**, 1 (1979); (b) A. B. Harris, S. Kim, and T. C. Lubensky, Phys. Rev. Lett. **53**, 743; **54**, 1088(E) (1984).
[22]J. E. de Oliveira and H. M. Rosenberg, unpublished results, as cited in Ref. 18.
[23]J. A. Krumhansl, Phys. Rev. Lett. **56**, 2696 (1986).
[24]*Amorphous Solids*, edited by W. A. Phillips (Springer-Verlag, Berlin, 1981).
[25]A. C. Meeks, Polymer **15**, 675 (1974).
[26]P.-G. de Gennes, *Scaling Concepts in Polymer Physics* (Cornell University Press, Ithaca, NY, 1979); M. Doi and S. F. Edwards, *The Theory of Polymer Dynamics* (Clarendon, Oxford, 1986).
[27]T. Achibat, A. Boukenter, E. Duval, G. Lorenz, and S. Eti-

enne, J. Chem. Phys. **95**, 2949 (1991).
[28]L. M. Torell and S. Schantz, in *Polymer Electrolyte Reviews—2,* edited by J. R. MacCallum and C. A. Vincent (Elsevier, New York, 1988); L. M. Torell and C. A. Angell, Br. Polym. J. **20**, 173 (1988); S. Schantz, L. M. Torell, and J. R. Stevens, J. Appl. Phys. **64**, 2038 (1988); L. Börjesson, J. R. Stevens, and L. M. Torell, Polymer **28**, 1803 (1987).
[29]D. A. Jennings and H. Takuma, Appl. Phys. Lett. **5**, 241 (1964).
[30]E. S. Stewart and J. S. Stewart, Phys. Rev. Lett. **13**, 437 (1964).
[31]D. A. Pinnow, S. J. Candau, J. T. LaMacchia, and T. A. Litovitz, J. Acoust. Soc. Am. **43**, 131 (1967).
[32]R. D. Mountain, J. Res. Natl. Bur. Stand. A **70**, 207 (1966); Rev. Mod. Phys. **38**, 205 (1966).
[33]B. J. Berne and R. Pecora, *Dynamic Light Scattering* (Wiley, New York, 1976).
[34]C. J. Montrose, V. A. Solovyev, and T. A. Litovitz, J. Acoust. Soc. Am. **43**, 117 (1967).
[35]L. Börjesson, L. M. Torell, and W. S. Howells, Philos. Mag. B **59**, 105 (1989).
[36]S. D. Druger, A. Nitzan, and M. A. Ratner, J. Chem. Phys. **79**, 3133 (1983); S. D. Druger, M. A. Ratner, and A. Nitzan, Solid State Ionics **9/10**, 1115 (1983); Phys. Rev. B **31**, 3939 (1985); R. Granek, A. Nitzan, S. D. Druger, and M. A. Ratner, Solid State Ionics **28-30**, 120 (1988).
[37]G. S. Grest, I. Webman, S. A. Safran, and A. L. R. Bug, Phys. Rev. A **33**, 2842 (1986); A. L. R. Bug and Y. Gefen, *ibid.* **35**, 1301 (1985).
[38]A. K. Harrison and R. Zwanzig, Phys. Rev. A **32**, 1072 (1985).
[39]R. Granek and A. Nitzan, J. Chem. Phys. **90**, 3784 (1989); **93**, 5918 (1990).
[40]T. Odagaki and M. Lax, Phys. Rev. B **24**, 5284 (1981).
[41]I. Webman, Phys. Rev. Lett. **47**, 1496 (1981).
[42]S. Summerfield, Solid State Commun. **39**, 401 (1981).
[43]M. Sahimi, B. D. Hughes, L. E. Scriven, and H. T. Davis, J. Chem. Phys. **78**, 6849 (1983).
[44]A. A. Maradudin, E. W. Montroll, G. H. Weiss, and I. P. Ipatova, *Theory of Lattice Dynamics in the Harmonic Approximation* (Academic, New York, 1971).
[45]N. W. Ashcroft and N. D. Mermin, *Solid State Physics* (CBS Publishing Asia, Philadelphia, 1976).
[46]P. Bruesch, *Phonons: Theory and Experiment I,* Vol. 34 of *Springer Series in Solid State Sciences* (Springer-Verlag, New York, 1982).
[47]Y. Kantor and I. Webmann, Phys. Rev. Lett. **52**, 1891 (1984); I. Webman and G. S. Grest, Phys. Rev. B **31**, 1689 (1985); D. J. Bergman, *ibid.* **31**, 1671 (1985); **33**, 2013 (1986); K. Yakubo and T. Nakayama, in *Phonons 89* (Ref. 11).
[48]Equations (44) and (45) imply that for this regime of small ω and τ^{-1}, $K \sim p - p_c \ll 1$ is a self-consistent solution; hence $|\varepsilon| \sim p - p_c \ll 1$.
[49]P. G. Klemens, Proc. R. Soc. London A **208**, 108 (1951).
[50]Lord Rayleigh, *Theory of Sound* (MacMillan, London, 1896), Vol. 2; L. D. Landau and E. M. Lifshitz, *Fluid Mechanics* (Pergamon, Oxford, 1986), Sec. 76.
[51]Note that the factor $n(\omega)+1$, which is frequency dependent, is also left out. $\mathrm{sgn}(\omega)$ is the signum function and is included in Eq. (62) since $n(-\omega)+1=-n(\omega)$, thus keeping $S(q,\omega)$ positive for negative ω.
[52]For the full scattered intensity [Eq. (59)], symmetry between the peaks is not generally present because of the $n(\omega)+1$ factor, $n(-\omega)+1=-n(\omega)$. In the classical limit ($\hbar\omega \ll k_B T$), $n(\omega)+1 \simeq k_B T/\hbar\omega$ and the peaks are approximately symmetrical.
[53]A. F. Ioffe and A. R. Regel, Prog. Semicond. **4**, 237 (1960).
[54]N. F. Mott, Philos. Mag. **19**, 835 (1969).
[55]Actually, for polymeric materials the fractal picture is more suitable for the transverse than for the longitudinal phonons. The hard-core interactions between monomers should provide the dominant channel of propagation of the longitudinal phonons, and fractal effects may not be easily observed in experiment.
[56]For reviews, see M. A. Ratner and D. F. Shriver, Chem. Rev. **88**, 109 (1988); M. A. Ratner in *Polymer Electrolyte Reviews-1,* edited by J. R. MacCallum and C. A. Vincent (Elsevier, New York, 1987), p. 173.
[57]Dimensionless quantities are used here; the monomer length a can be used to obtain the correct dimensions.
[58]M. Soltwisch, J. Sukmanowski, and D. Quitmann, J. Chem. Phys. **86**, 3207 (1987).
[59]Except at very low temperatures (Ref. 24). At temperatures of ~ 10 K, a maximum in the sound velocity versus temperature curve usually appears, and the sound velocity decreases with decreasing temperature below that temperature (Ref. 24).
[60]J. K. Kruger and M. Pietralla, in *Order in the Amorphous "State" of Polymers,* edited by S. K. Keinath, R. L. Miller, and J. K. Rieke (Plenum, New York, 1987); J. K. Kruger, Solid State Commun. **30**, 43 (1979).
[61]H. Vogel, Z. **22**, 645 (1921); G. Tammann and W. Heese, Z. Anorg. Allg. Chem. **156**, 245 (1926); G. S. J. Fulcher, Am. Ceram. Soc. **8**, 339 (1925).
[62]E. Leuthesser, Phys. Rev. A **29**, 2765 (1984); M. Elmroth, L. Börjesson, and L. M. Torell, Phys. Rev. Lett. **68**, 79 (1992).
[63]R. Kubo, Adv. Chem. Phys. **15**, 101 (1969).
[64]N. O. Birge, Phys. Rev. B **34**, 1631 (1986), and references therein.